

Small-scale model testing of cyclically axially loaded piles

Santiago de Veloza Coelho Correia Pinto

Dissertation to obtain the Master of Science Degree in

Civil Engineering

Supervisors

Professor Doctor Peter John Bourne-Webb

Professor Doctor Jaime Alberto dos Santos

Examination Committee

Chairperson: Professor Doctor Orlando José Barreiros d'Almeida Pereira

Supervisor: Professor Doctor Peter John Bourne-Webb

Member of Committee: Professor Doctor Luís Manuel Calado de Oliveira Martins

June 2022

Declaration

I declare that this document is an original work of my own authorship and that it fulfills all the requirements of the Code of Conduct and Good Practices of the Universidade de Lisboa.

Acknowledgements

Firstly, I am thankful for FCT for funding and sponsoring this project, I am sincerely honored to have been selected as the recipient of a scholarship. Without it, none of this would not have been possible.

I would like to thank Professor Peter Bourne-Webb for giving me the opportunity of working on this subject, as well as for all the amazing support and guidance throughout the process.

Lastly, I would also like to express my gratitude to my family and to my friends Bé, Cátia Saudades, Nuno Machado, Patrícia Ganhão and Maria João Pupo Correia, for their full support throughout my academic path.

Abstract

Throughout the years, the need for heavier and more complex structures have stimulated the development of pile foundations, which may be subjected only to monotonic loading, but also to cyclic loading. However, the deterioration effects of cyclic loading have only been studied in the last five decades and these remain largely unknown. The offshore structures' foundations are often more susceptible to cyclic axial loading, driving the research in this field, where the addressed cyclic periods are relatively low. In that regard, this dissertation explored the overall cyclic pile-soil system behaviour when longer periods were considered, supporting the study of the long-term cyclic performance of energy piles.

This dissertation incorporated both theoretical and experimental publications review of existing studies around the cyclic pile-soil behaviour and while it is extensive, the parameters studied vary significantly from author to author. Featuring an experimental campaign in the framework of studying the effects of cyclic axial loading on piles, a small-scale pile and various equipment were used. Several variables were taken into account and the hypothesis of the increasing stiffening effect of a tensioned and compressed soil is made. The demystification about the soil initial state is discussed, being concluded it can be considered partly irrelevant, only after running a number of cycles. Lastly the pre-cycling is considered beneficial since it is a step further in the prediction of the cyclic pile-soil behaviour.

Keywords

Pile foundations; cyclic axial loading; shaft resistance degradation; small-scale testing

Resumo

Ao longo dos anos, a necessidade de estruturas de maior porte e complexidade estimulou o desenvolvimento de fundações em estacas, que podem estar submetidas apenas a carregamentos estáticos, assim como a carregamentos cíclicos. Não obstante, os efeitos de deterioração provenientes de cargas cíclicas apenas têm sido alvo de estudo nas últimas cinco décadas, permanecendo, em grande parte, desconhecidos. As fundações de estruturas *offshore* são frequentemente as mais suscetíveis a carregamentos axiais cíclicos, impulsionando a investigação neste campo, em que os períodos cíclicos abordados são relativamente baixos. Nesse sentido, este trabalho teve como objetivo explorar o comportamento cíclico geral do sistema solo-estaca, quando são considerados períodos mais longos, auxiliando ainda o estudo do desempenho cíclico a longo prazo de estacas energéticas.

Este trabalho incorporou ainda revisões teórica e experimental de publicações de estudos existentes sobre o comportamento cíclico do sistema solo-estaca e, embora seja extensa, os parâmetros estudados variam significativamente. Foi realizada uma campanha experimental no âmbito do estudo dos efeitos do carregamento axial cíclico em fundações por estacas, e utilizou-se uma estaca em pequena escala e diversos equipamentos. Distintas variáveis foram levadas em consideração e foi colocada uma hipótese acerca do efeito de rigidez crescente de um solo tensionado e logo após comprimido. Discute-se ainda a desmistificação sobre o estado inicial do solo, concluindo-se que pode ser considerado parcialmente irrelevante, após a execução de apenas alguns ciclos. Por fim, a pré-ciclagem do solo é considerada benéfica, pois representa um passo na direção da melhor previsão do comportamento cíclico do solo.

Palavras-Chave

Fundações por estacas; carregamento axial cíclico; degradação da resistência lateral; investigação em pequena escala

Table of Contents

- List of Figures ix
- List of Tables..... xi
- List of Abbreviations..... xii
- List of Symbols..... xii
- 1 Introduction 1
 - 1.1 Context and Motivation..... 1
 - 1.2 Objectives..... 2
 - 1.3 Dissertation outline 2
- 2 Pile Foundations 3
 - 2.1 Preliminaries..... 3
 - 2.2 Pile classification 4
 - 2.2.1 By ground conditions..... 4
 - 2.2.2 By installation method 5
 - 2.2.3 Energy Piles 9
 - 2.3 Pile axial loading..... 10
 - 2.3.1 Static load resistance 10
 - 2.3.2 Monotonic load-displacement behaviour..... 13
- 3 Piles under axial cyclic loading 15
 - 3.1 General context 15
 - 3.2 Characterisation of cyclic loads 16
 - 3.3 Concept of Cyclic Stability Diagram 17
 - 3.4 Effects of Cyclic Axial Loading and Influencing Factors 18
 - 3.4.1 Degradation of the shaft resistance..... 19
 - 3.4.2 Influence of installation method..... 22
 - 3.5 Design of Cyclically Axially Loaded Piles 22
 - 3.6 Full-scale cyclic axial load testing of piles 23
 - 3.6.1 Plancoët, near St. Malo, France..... 23
 - 3.6.2 Loon-Plage, near Dunkirk, France, 25
 - 3.7 Small-scale cyclic axial load testing of piles 25
 - 3.7.1 Small-scale testing fundamentals..... 25
 - 3.7.2 Blanc et al. (2015) 26
 - 3.8 Summary of Experimental Case Studies 27
- 4 Materials and methods 29
 - 4.1 Equipment 29
 - 4.1.1 Small-scale model pile 29
 - 4.1.2 Stepper Motor..... 30

4.1.3	Potentiometric Position Transducer (POPT)	32
4.1.4	Load Cell	33
4.1.5	Data Acquisition Hardware and Software (Data logger).....	33
4.1.6	Tank	34
4.2	Materials: Soil	35
4.2.1	Particle size distribution.....	37
4.2.2	Particle density, ρ_s	37
4.2.3	Minimum dry density / unit weight	38
4.2.4	Maximum dry density / unit weight	39
4.3	Soil sample preparation methodology	39
4.4	Sensor calibration	41
4.4.1	Displacement transducer.....	42
4.4.2	Load cell	42
4.5	Pile testing methodology	43
5	Test results & Discussion	45
5.1	Monotonic load response	46
5.1.1	Estimation of monotonic ultimate load, according to the EN 1997-1.....	46
5.1.2	MON/C-1, T-1 & C-2.....	47
5.1.3	MON/T-2, C-3 & T-3	50
5.1.4	MON/T-4 & C-4	51
5.2	Cyclic load response: effect of soil initial state	53
5.2.1	Dense sand cyclic tests.....	53
5.2.2	Loose sand cyclic tests	59
6	Conclusions & Recommendations.....	63
6.1	Conclusions.....	63
6.2	Recommendations for future work.....	64
	References.....	66
	Appendices	1
	Appendix A – Checklist for Running the Tests	A
	Appendix B – Small scale pile schematic view and dimensions	B
	B	
	Appendix C – APAS 30 Supplier Technical Sheet	C
	Appendix D – Particle Size Testing (Standard E 239)	D
	Appendix E – Particle density testing.....	E

LIST OF FIGURES

Figure 1 - Flowchart of different installation pile methods	3
Figure 2 - (a) End-bearing Pile and (b) Friction Pile	4
Figure 3 - Bored pile installation sequence, El Haffar (2018)	5
Figure 4 - CFA Pile installation procedure, as per Keller UK Limited	6
Figure 5 - (a) Pile being driven into position; (b) Driven Piles, as per Keller UK Limited	7
Figure 6 - Pile Jacking technique, as per Keller USA Limited	8
Figure 7 - Energy Piles and seasonal thermal loading cycles, Brandl (2006)	9
Figure 8 - (a) Pile in compression; (b) Pile in tension	10
Figure 9 - EN 1997-1 three-step process to determine the pile design resistance	12
Figure 10 - Load-Displacement curve for compressive load to failure on pile, adapted from Tomlinson & Woodward (2008)	13
Figure 11 - Simple representation of the mobilisation of the resistances on a Load-Displacement curve for (a) replacement piles and (b) displacement piles	14
Figure 12 - Periods and number of cycles of typical cyclic loading events, Andersen et al. (2013).....	15
Figure 13 - Cyclic axial loading variables, Jardine & Standing (2012).....	16
Figure 14 - Cyclic Stability Diagram, Poulos (1988)	17
Figure 15 - Results from model tests with monotonic and cyclic loading, Poulos (1991)	19
Figure 16 - Conceptual Model of pile-soil interface friction, Fioravante (2002)	19
Figure 17 - Friction Fatigue mechanism proposed by White and Bolton (2002).....	21
Figure 18 - Particles tendency to crush when submitted to cyclic loading.....	21
Figure 19 - Pile head displacements(z)-Number of cycles (N) curve, Puech & Jezequel (1981).....	24
Figure 20 – Sketch of Cyclic Stability Diagram based on Puech & Jezequel (1981) results .	24
Figure 21 - Cyclic Stability Diagram, adapted from Blanc et al. (2015)	27
Figure 22 - Laboratory Test Setup	29
Figure 23 - Small scale Pile and its texture.....	30
Figure 24 - Detail of Motor-Frame and Motor-Pile connection.....	31
Figure 25 - POPT (a) return spring mechanism and (b) in place prior to test.....	32
Figure 26 - (a) View of Data Logger and (b) Internal view of iNet-412 wiring box	33
Figure 27 - InstruNet-W+ control software interface capturing (a) load and (b) displacement vs time plots in real-time	34
Figure 28 - Initial tests graphs: a) load-time, b) displacement-time and c) load-displacement (units in N, s and mm).....	34
Figure 29 - (a) Tank used for the experimental campaign; (b) Tank dimensions	35

Figure 30 - APAS 30 Sand.....	36
Figure 31 - Particle size distribution curve for APAS 30	37
Figure 32 - Particle density test materials and equipment.....	38
Figure 33 - (a) Sampling cups for sand density control and (b) dimensions.....	39
Figure 34 - Sampling cups for sand density control put in place	40
Figure 35 - Funnel and tube used for a loosened sand preparation.....	41
Figure 36 - POPT calibration using a micrometre.....	42
Figure 37 - Schematic of laboratory setup.....	44
Figure 39 - (a) Load-Time and (b) Displacement-time graphs, MON/C-1.....	47
Figure 40 - MON/C-1 Test (a) Displacement-load plot and (b) close-up	47
Figure 41 - MON/T-1 Test Displacement-load graph.....	48
Figure 42 - MON/C-2 Test Displacement-load graph	48
Figure 43 - Conjecture of soil behaviour between MON/T-1 and MON/C-2	49
Figure 44 – (a) MON/T-2 and (b) MON/T-3 Test Displacement-load graphs.....	50
Figure 45 - MON/C-3 Test Displacement-load graph	51
Figure 46 - MON/T-4 Test Displacement-load graph.....	51
Figure 47 - MON/C-4 Test Displacement-load graph	52
Figure 48 - Displacement-time graph for CYC/TC-1.....	54
Figure 49 - Load-time graph for CYC/TC-1.....	55
Figure 50 - Load-Displacement graphs for tests CYC/TC-1 through 4 in dense sand	55
Figure 51 - Variations in maximum attained loads on dense sand test	57
Figure 52 - Load-displacement curves for CYC/TC: 2 & N=3 (left) and 4 & N=2 (right)	58
Figure 53 - Load-Displacement graphs for tests CYC/TC-5 through 8 in loose sand.....	60
Figure 54 - Variations in maximum attained loads on loose sand	61
Figure 55 - Load-Displacement at N = 10 for tests CYC/TC-5 through 8	61

LIST OF TABLES

Table 1 - Pile shaft and base resistance calculations, Santos (2008)	11
Table 2 - Test results, by Benzaria et al. (2013).....	25
Table 3 - Scaling factors for different parameters.....	26
Table 4 - Small-scale test results, Blanc et al. (2015).....	26
Table 5 - Summary table of experimental literature review.....	28
Table 6 - Reference values for the equivalence between required displacement a stepper motor steps (409600 steps per 5.08 mm).....	31
Table 7 - APAS 30 soil parameters.....	36
Table 8 - Sand unit weights obtained in sample preparation trial	41
Table 9 - Summary of the model pile tests executed, in chronological order	44
Table 10 - Summary details of model pile tests executed	45
Table 11 - Model parameters and ultimate load estimation according to the EN 1997-1	46
Table 12 - Sequence of motor commands for CYC/TC-1 through 4.....	54
Table 13 - Variations in attained loads and displacement on dense sand preliminary tests .	58
Table 14 - Variations in attained loads and displacement on loosen sand preliminary tests.	61

LIST OF ABBREVIATIONS

ASTM	American Society for Testing and Materials
CFA	Continuous Flight Auger
CPT	Cone Penetration Test
FS	Factor of Safety
NP	Portuguese Standard
PMT	Pressuremeter Test
POPT	Potentiometric Position Transducer

LIST OF SYMBOLS

Latin Alphabet

A_b	Cross-sectional area of the pile base
A_s	Surface area of the pile in contact with soil
C_u	Coefficient of uniformity
$\bar{c}_{u,i}$	Average undrained soil shear strength along the pile
$c_{u,b}$	Average undrained shear strength at the pile base
d_{10}	Particle size at which 10% of the particles in sample are smaller
d_{50}	Particle size at which 50% of the particles in sample are smaller
d_{60}	Particle size at which 60% of the particles in sample are smaller
D	Pile diameter
D_r	Soil relative density
e_{\max}	Maximum void ratio
e_{\min}	Minimum void ratio
f	Cyclic frequency
g	Gravitational acceleration

G	Strain and pressure dependent shear modulus of soil
G_s	Specific Gravity
HW i	Sampling cup placed half-way up no. i
B i	Sampling cup placed in the bottom no. i
N	Number of cycles
N_a	Intensity of the acceleration of model (Model factor)
N_f	Number of cycles necessary to failure
N_c	Bearing capacity factor
N_q	Bearing capacity factor
k_1	"Elastic spring" stiffness
K	Coefficient of lateral stress
L	Pile length
Q_{cyclic}	Axial cyclic axial load amplitude increment
Q_{max}	Peak maximum load
Q_{mean}	Mean load
Q_{min}	Peak minimum load
$Q_{ult,c}$	Ultimate monotonic compression load
$Q_{ult,t}$	Ultimate monotonic tension load
R	Pile radius
R_b	Ultimate base resistance
$R_{c;u}$	Axial ultimate resistance in compression
$R_{t;u}$	Axial ultimate resistance in tension
R_s	Ultimate shaft resistance
R_k	Characteristic pile resistance
R_u	Axial ultimate resistance (either in tension or in compression)
T	Cyclic period
z	Pile head displacement

Greek Alphabet

α	Adhesion factor
γ	Partial safety factor
γ_d^{\max}	Maximum dry unit weight
γ_d^{\min}	Minimum dry unit weight
σ'_n	Normal effective stress to the pile-soil interface
$\bar{\sigma}'_v$	Mean vertical effective stress along the pile
$\sigma'_{v,b}$	Vertical effective stress at the pile base level
Δu	Displacement normal to the pile shaft
δ	Angle of friction at the soil-pile interface
ρ_s	Particle density
ξ	Correlation factor

1 INTRODUCTION

1.1 CONTEXT AND MOTIVATION

Throughout the years, the need for heavier and more complex structures have stimulated the development of pile foundations, which have proven to be of great efficacy. This type of foundations is principally used to transfer the loads from the superstructure onto deeper and less compressible soil strata, gaining resistance properties unavailable near the surface.

Up until 50 years ago, pile foundations used to be designed considering the applied load to be only static. This, however, has proven to be limitative, since the load can also be cyclic, especially on offshore structures, which are now acknowledged to handle cyclic loads more often than in onshore ones. This type of loading is recognised for having a negative impact on the resistance and performance of a pile foundation, since its capacity is notoriously reduced when under cyclic loads. The most common and noteworthy phenomenon is the degradation of the resistance mobilised along the shaft of the pile, which may trigger failure leading to large and uncontrollable displacements. Although the importance of taking into account this type of loading and its resistance deteriorative properties are recognised, the European structural design code for geotechnical structures, EN 1997-1, reveals no approach or instruction on how to consider its effects, other than *severe adverse effect of cyclic loading (...) shall be considered*.

In the framework of considering cyclic loads, numerous experimental research has been devoted to it by various authors; nonetheless, the periods of loads considered in existing studies suggests that little has been done to address longer periods and large numbers of cycles. In that regard, this work explores the overall cyclic pile-soil behaviour when longer periods of mechanical loading were considered, and it was intended to support the study of the long-term cyclic performance of energy piles. These piles are submitted to cyclic thermal loading as a result of being exposed to daily (i.e., day and night) and seasonal (i.e., summer and winter) temperature variations during their lifetime, which may cause axial displacements and additional axial stresses.

This dissertation incorporates both theoretical and experimental literature review of existing studies around cyclic pile-soil behaviour and while it is extensive, the parameters studied vary significantly from author to author. The dissertation also features an experimental campaign in the framework of studying the effects of cyclic axial loading on piles, where a small-scale pile and various equipment were used. Several variables were taken into account and possible conjectures are discussed.

1.2 OBJECTIVES

This dissertation is driven by the experimental study of the cyclic axial loading effects on piles and its importance therefore, numerous objectives were targeted to be achieved, namely:

- Based on a theoretical literature review, identify the main concerns of the cyclic pile-soil behaviour;
- Based on an experimental literature review, create a database of existing cyclic axial load tests on pile foundations;
- Undertake geotechnical classification and element testing of the test soil;
- In the framework of the experimental campaign: familiarise with the data acquisition and control software;
- Finalise the equipment development, calibration and methodology;
- Undertake static mechanical load tests to confirm pile resistance, considering different initial soil states;
- Plan and undertake a test program to generate the cyclic stability framework for the model pile-soil system under cyclic loading.

1.3 DISSERTATION OUTLINE

This dissertation is organized in six Chapters. In this Chapter 1, a general overview of the problematic of piles under cyclic axial loading is presented, the main objectives are listed and the document organisation is described.

The following two chapters focus on the literature review. In Chapter 2, the preliminaries about the different pile types are described, as well as the monotonic/static load-displacement behaviour is depicted. Chapter 3, on the other hand, focuses on the literature review of piles under axial cyclic loading, the cyclic parameters are discussed, the concept of Cyclic Stability Diagram is introduced and full-scale and small-scale experimental literature are examined.

In Chapter 4, the entire laboratory setup for the experimental campaign is described, including the geotechnical classification and testing is performed to the soil used. This Chapter focuses on illustrating the laboratory equipment preparation before running tests.

In Chapter 5, based on the previous Chapters, the experimental campaign took place and several tests were run, varying the soil state conditions and other cyclic parameters.

Finally, in Chapter 6, the main conclusions of the research are presented and some recommendations for future developments are suggested.

2 PILE FOUNDATIONS

2.1 PRELIMINARIES

Pile foundations are principally used to transfer the loads from superstructures, through weak and/or compressible strata onto stronger and stiffer geological formations, possibly several tens of meters below the soil surface. In other words, pile foundations are commonly used for building foundations to transfer load to deeper layers of soil or rock, that have improved bearing capacity as well as acceptable settlement behaviour. It is thought that piling techniques date back to, at least, the 4th Century BC and, in its earliest form, a pile foundation consisted of rows of timber stakes driven into the ground to support overlying structures. Over the years, the increasing demand for taller and heavier structures has led to the growing use of foundation piles. This type of deep foundation has allowed mankind to design more complex structures, and it has proven great efficacy. Depending on the equipment used, ground conditions and method of installation, different pile types are distinguished.

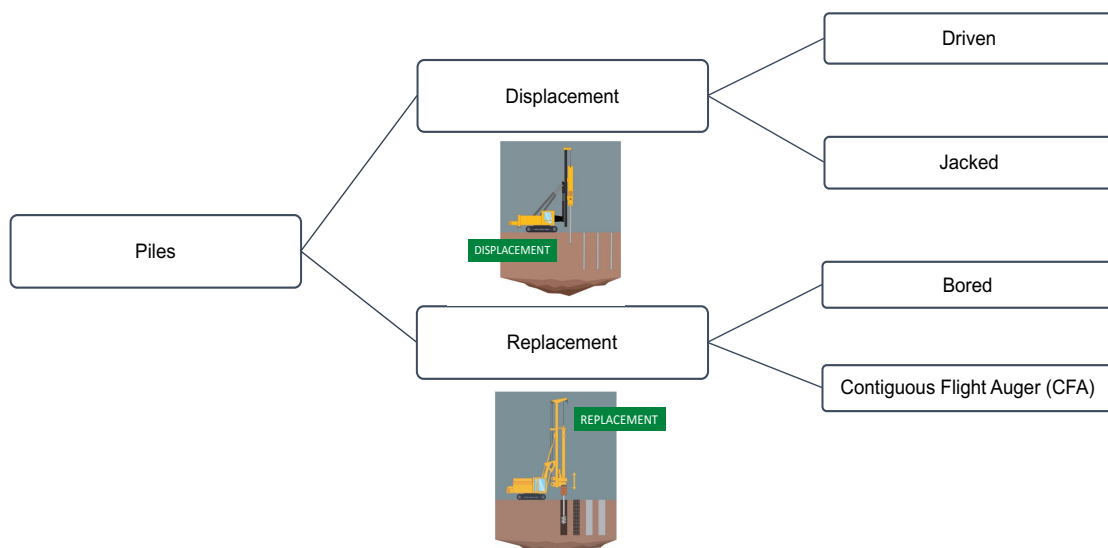


Figure 1 - Flowchart of different installation pile methods

Even though it is adequate, in many situations, to categorise the various types of pile and their method of installation, using a simple division into 'driven' or 'bored' piles, it does not satisfactorily cope with the many different forms of pile now in use. Therefore, a more rigorous division into 'displacement' or 'replacement' piles overcomes this difficulty, as some piles are installed by a combination of these methods and their description may require qualification (Fleming et al., 2020). Thus, depending on the method of installation and its effects in terms of the impact of installation on the surrounding soils, two main pile classifications can be identified: Displacement and Replacement piles.

The term Displacement Pile is generally used when piles are inserted in the ground by jacking, impact driving or even vibrating, which leaves the soil in place, but pushes it out of the way. On the other hand, Replacement Piles are formed by excavating the ground to provide a void in which the pile is constructed. A flowchart with the different subcategories of piles is shown in Figure 1.

2.2 PILE CLASSIFICATION

Different pile types can be classified not only by their installation method, but also by the ground conditions and consequent developed load-bearing capacities.

2.2.1 By ground conditions

Two major groups are identified when categorising piles according to the ground conditions, which are: End-bearing and Friction piles. Though the names are self-explanatory, the main difference between the two classifications mentioned lies on which part of the pile, i.e. base or shaft, the most load-bearing capacity is developed (Yasufuku et al., 2001).

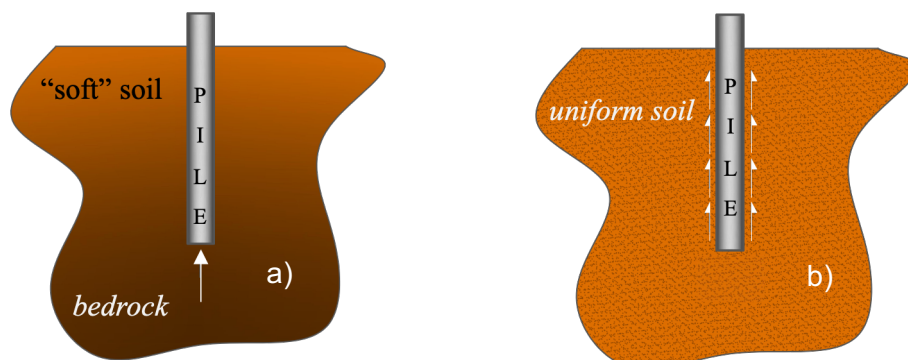


Figure 2 - (a) End-bearing Pile and (b) Friction Pile

End-bearing piles develop most of their load-bearing capacity at the base of the pile. This type of piles transmits the load through soft and highly compressible soil onto rock or hard relatively incompressible soil, sometimes known in engineering jargon as the *bedrock*, as shown in Figure 2.a). On the other hand, Friction piles develop most of the load-bearing capacity along the sides of the pile. The whole surface of the pile works to transfer the forces to the surrounding soil, as shown in Figure 2.b). In Friction piles, the longer is the depth into the ground, the more load the pile can support – the load-bearing capacity of the pile is directly proportionate to its length. For this reason, this is applicable to cases where the soil conditions are not very firm, but so long the pile length is enough to provide the required resistance.

In conclusion, friction piles are in contrast to end-bearing piles, which rely primarily on the mobilised resistance at the base of pile since it is where the soil conditions are firmer. While

Friction piles rely mostly on the mobilised resistance along the pile-soil interface, having a bearing capacity as great as their embedded length.

2.2.2 By installation method

According to their installation procedure, different types of piles can be identified.

2.2.2.1 Bored Piles

The installation of bored piles is a replacement technique, meaning the installation process consists of soil removal to accommodate the pile. In its construction process, a hole is drilled on the ground, with or without the use of additional side support (casing and/or fluids), in which steel reinforcement is positioned and concrete is cast, as shown in Figure 3.

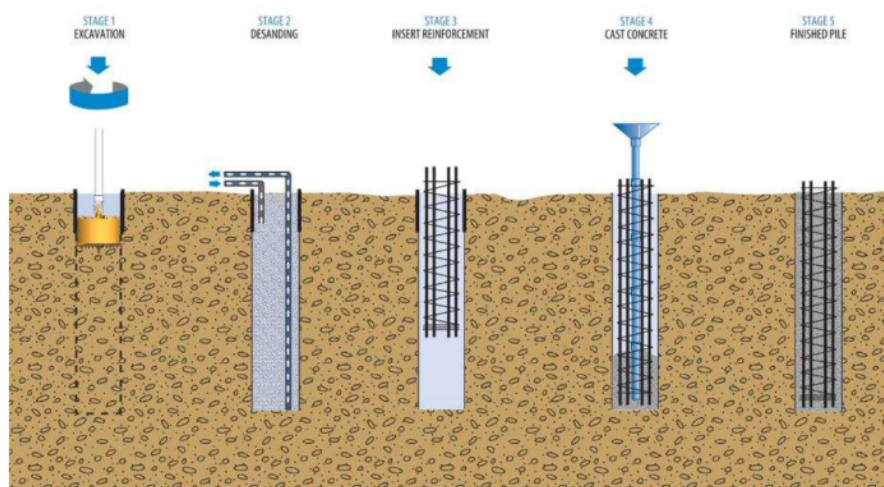


Figure 3 - Bored pile installation sequence, El Haffar (2018)

Bored piles are used primarily in cohesive subsoils for the formation of friction piles, and when pile foundations are close to existing buildings. Among various advantages, the following are highlighted:

- The length can readily be varied to adapt to variations in levels of bearing stratum;
- Great depths and diameters can be achieved (record of 150 m);
- The soil/rock removed during boring can be inspected for comparison with site investigation data;
- It can be installed without appreciable noise or vibration, hence being popular in urban areas;
- The material forming pile is not governed by handling or driving stresses.

On the other hand, the main disadvantages are:

- The concrete located in the shaft is liable to squeezing in soft soils;

- The concrete cannot be inspected after installation;
- In unstable soils, casing is necessary;
- Special techniques are needed for concreting in water-bearing soils.

2.2.2.2 Continuous Flight Auger Piles (CFA)

The Continuous Flight Auger (CFA) pile is also considered a replacement pile because soil extraction takes place before constructing the pile. What differs, though, is the construction process. The concrete casting is achieved by pumping fluid concrete through the hollow stem of a helical screw, or auger, at the same time as the auger starts being pulled out of the ground. Then, the steel reinforcement is immediately placed after the auger is out of the ground, while the concrete is still fluid enough, Figure 4.

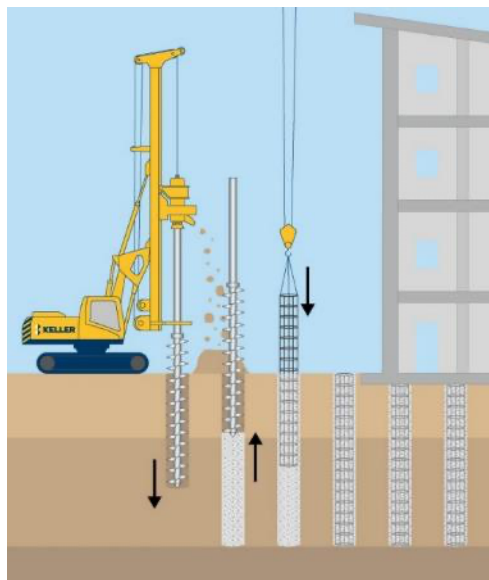


Figure 4 - CFA Pile installation procedure, as per Keller UK Limited

In Gavin et al., (2008), it is indicated that CFA piles are a very efficient solution, depending mainly on the pile geometry, soil conditions and also on how they are drilled. In CFA piles, there is a balance to be achieved between drilling “tight” (which would be considered more of a displacement type) and wear-and-tear on the augers due to the force required to push them into the ground. It is recommended to avoid drilling too loose, as this can lead to very poor outcomes in terms of pile resistance. Generally, high quality CFA piles need on board instrumentation to monitor the process, due its high uncertainties.

The average pile shaft resistance, R_s , is comparable to that mobilised by driven piles. A physical explanation for the enhanced shaft resistance of CFA piles is that the piles are unaffected by the phenomenon of friction fatigue, which occurs during the installation of driven

piles. Regarding the mobilised base resistance, R_b , on a highly controlled CFA pile, it can be twice to 3 times what would be tolerable on a bored pile, and even comparable to a driven pile.

Among various advantages, the following are highlighted (Fleming et al., 2020):

- The process is quick and less costly, when compared to other installation methods;
- This method of pile construction is suitable in a wide range of soils, namely in sands, gravels and clays;
- In unstable soils, there is no need for casing or fluid to support the soil, as the bored piles would need, even in high water table situations;
- It offers considerable environmental advantages during construction;

On the other hand, the main disadvantages are:

- The length is limited to 30-35 m as well as the diameter is to 1.2 m;
- It requires a strict control of the relative rates of auger extraction and concrete intrusion;
- it is not possible to check the stratification and quality of the soil during installation as with conventional bored piles. This is particularly required where a high proportion of the load is carried in end-bearing;
- In certain ground conditions, doubts may exist as to whether or not the injected material has flowed-out to a sufficient extent to cover the whole drilled area.

2.2.2.3 Driven Piles

Driven piles, as the name suggests, consist of driving a pile into the ground with a driving machine, as shown in Figure 5 a) and b). Consequently, it is considered a displacement method because the soil is pushed out of the way of its path, displacing it radially during installation. Due to their driving technique driven piles are, generally, either prefabricated concrete or steel profile.

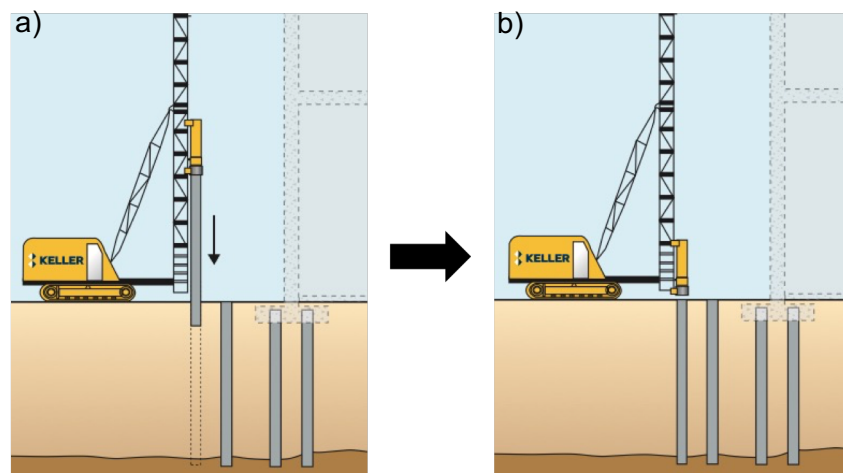


Figure 5 - (a) Pile being driven into position; (b) Driven Piles, as per Keller UK Limited

Driven piles are used primarily in marine and river structures, since it is impracticable to cast in situ piles, as well as when the ground conditions are more favourable to this type of piles i.e., very soft clays or loose granular soils. While in onshore structures both driven and bored piles can be used, in offshore structures driven piles are predominant.

Among various advantages, the following are highlighted:

- Material forming pile can be inspected for quality and soundness before driving;
- Not liable to 'squeezing', since it is not cast-in-situ;
- Construction operations not affected by groundwater;
- Unlike displacement piles, there is no soil waste to be disposed of;
- Suitable for non-cohesive soils.

On the other hand, the main disadvantages are:

- It may break during driving, necessitating to be replaced;
- The noise and ground vibration due to driving may be unacceptable, especially in urban areas;
- It can be limited by hard ground and less powerful equipment;
- The displacement of soil during driving may damage adjacent structures;
- These piles cannot be driven in conditions of low headroom.

2.2.2.4 Jacked Piles

Jacked piles are also considered as a displacement pile, in which the aspect that changes is the method by which the installation energy is provided. These piles are constructed using small-diameter piles that are jacked by hydraulic jacks, which make use of an existing structure as a reaction for jacking the piles, as shown in Figure 6.



Figure 6 - Pile Jacking technique, as per Keller USA Limited

In this construction process, the structure is used as the reaction load and a hydraulic jack is used to push the pile into the ground. After reaching the required depth, the top of the pile is bracketed to the footing of the structure. The most common use for jacked piles is underpinning and increasing the load-bearing capacity of existing foundations, as shown in Figure 6.

This difference in installation method does seem to affect particularly the mobilised shaft resistance, R_s , since it is generally stiffer and stronger than that of driven piles (about 2x stiffer) and bored piles (about 10x stiffer). Whereas the base resistance, R_b , of jacked piles is weaker than that of driven piles (Fellenius, 2007). This technique has the advantage of being quieter than driving and almost vibration-less and there is no soil waste to be disposed of. However, compared to driven piles, jacked pile behaviour remains poorly understood and little research has been devoted to the comparison of their respective capacities (El Haffar, 2018).

2.2.3 Energy Piles

As aforementioned, this dissertation aimed supporting the study of the long-term cyclic performance of energy piles, by exploring the overall mechanical cyclic pile-soil system behaviour and considering longer cyclic periods.

The main purpose behind the use of energy piles is to enable the exploitation of geothermal energy for meeting the heating/cooling demands of buildings in an efficient and environment-friendly manner (Sutman et al., 2020). Therefore, energy pile is an energy geotechnical structure that couples a ground heat exchanger with a pile, making use of the energy stored as heat in the ground. These piles are submitted to months or years-long periods of cyclic thermal loading, which results in thermally induced cyclic stresses, (Brandl, 2006).

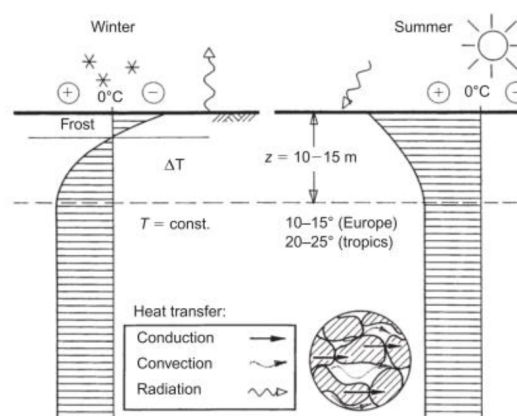


Figure 7 - Energy Piles and seasonal thermal loading cycles, Brandl (2006)

The thermal cyclic loading in energy piles arise, mainly, as a result of being exposed to daily (i.e. day and night) and seasonal (i.e. summer and winter) temperature variations during their lifetime, Figure 7. Therefore, these temperature cycles may cause axial displacements,

additional axial stresses, and changes in the resistance of the pile, with a daily and seasonal cyclic nature, along their lengths.

Concluding, the aim of this dissertation was to study the effects of long-term mechanical cyclic loading on piles and, while it supports cyclic performance of energy piles, the investigation of energy piles was not, however, the main goal of this study.

2.3 PILE AXIAL LOADING

2.3.1 Static load resistance

Axial loading of piles may be either compression or tension and there are a number of ways in which the load resistance may be established. There are two ways to estimate the resistances: (1) by calculation of the shaft and base resistance components, or (2) by measuring it directly through undertaken static and/or dynamic load testing. These resistances depend highly on the soil conditions, specifically: in cohesive soils, the shaft capacity is generally dominant, while in non-cohesive soil the overall capacity can be more evenly divided between shaft and base (Fleming et al., 2020).

Based on the equilibrium of vertical forces in Figures 8.a) and 8.b), the equations Eq. 2.1 and Eq 2.2 can be used to evaluate the ultimate compression and tension resistance, respectively.

$$R_{c;u} = R_b + R_s \quad (2.1)$$

$$R_{t;u} = R_s \quad (2.2)$$

Where:

$R_{c;u}$ is the axial ultimate resistance in compression;

$R_{t;u}$ is the axial ultimate resistance in tension;

R_s is the ultimate shaft resistance;

R_b is the ultimate base resistance.

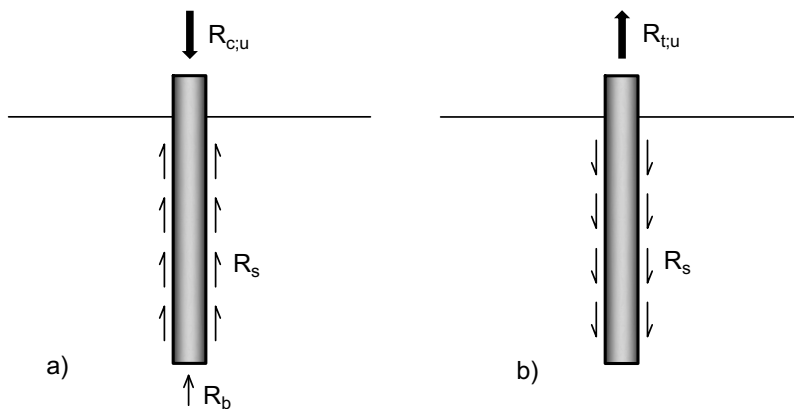


Figure 8 - (a) Pile in compression; (b) Pile in tension

To evaluate the pile ultimate resistance by calculation, an estimate of each resistance component is required. This may be done either by direct correlation with *in-situ* tests such as the cone penetration test (CPT) or pressuremeter (PMT), or by semi-empirical methods such as those summarised in Table 1.

The α -method is primarily used in clayey soils for which an undrained shear strength can be obtained while the β -method is mainly associated with granular soils, where the angle of shearing resistance can be obtained directly or indirectly but can also be used for clayey soils.

In these calculations, the empirical factors, K_s and α , are used to define the shaft resistance and are defined based on load testing of similar pile types under analogous loading and ground conditions. The bearing capacity factors, N_c & N_q , are derived from the *Theory of the Plasticity*, based on the surrounding soil characteristics and the geometric properties of the pile (Santos, 2008).

Table 1 - Pile shaft and base resistance calculations, Santos (2008)

Resistance component	Unit resistance, q_s / q_b	
	α -method (undrained conditions)	β -method (drained conditions)
Shaft: $R_s = \sum q_{s,i} \times A_{s,i}$	$\alpha_i \bar{c}_{u,i}$	$K_{s,i} \tan \delta_i \bar{\sigma}'_{v,i}$
Base: $R_b = q_b \times A_b$	$N_c c_{u,b}$	$N_q \cdot \sigma'_{v,b}$

Where:

A_b is the cross-sectional area of the pile base

A_s is the surface area of the pile in contact with soil

$\bar{c}_{u,i}$ is the average undrained shear strength in each fine-grained soil layer along the pile

$c_{u,b}$ is the average undrained shear strength at the pile base

N_c, N_q are bearing capacity factors

K is the coefficient of lateral stress

$\bar{\sigma}'_v$ is the mean vertical effective stress in each granular soil layer along the pile

$\sigma'_{v,b}$ is the vertical effective stress at the pile base

δ is the angle of friction at the soil-pile interface

α is the adhesion factor

According to the Eurocode 7, the ultimate resistance can be estimated based on analytical or empirical calculation methods whose validity has been demonstrated through static load tests in comparable situations, like the one explained in Table 1. Considering the method detailed in the code, the characteristic resistance values are evaluated.

Further, it is well known that geotechnical engineering is strongly associated with large uncertainties, because models are simplifications of complex real-world phenomena, being thus an important aspect to consider on the design process. Among many authors, Dithinde et al. (2011) considers two main sources of uncertainties as far as pile design by calculation is concerned, which are: (1) uncertainties associated with the calculation model input parameters, i.e. soil parameters, and (2) the uncertainty associated with the calculation model itself. This implies that soil parameters mentioned in Table 1, used on calculation models of the mobilised resistances, R_s and R_b are subject to these uncertainties and therefore interfere significantly in the results.

In acknowledgement of the importance of the model uncertainty, the European standards for geotechnical design, Eurocode 7 EN 1997-1, recommends that, when determining the design pile bearing capacity with a theoretical calculation model, partial factors must be introduced to ensure that the resistance obtained is sufficiently safe. Reference values of partial factors are set by national annexes, meaning each participating state has the power to choose the degree of uncertainty with which they are comfortable. Furthermore, a series of factors are suggested in the codes, and the calculation approach for obtaining design resistances are summarised step-by-step in Figure 9.

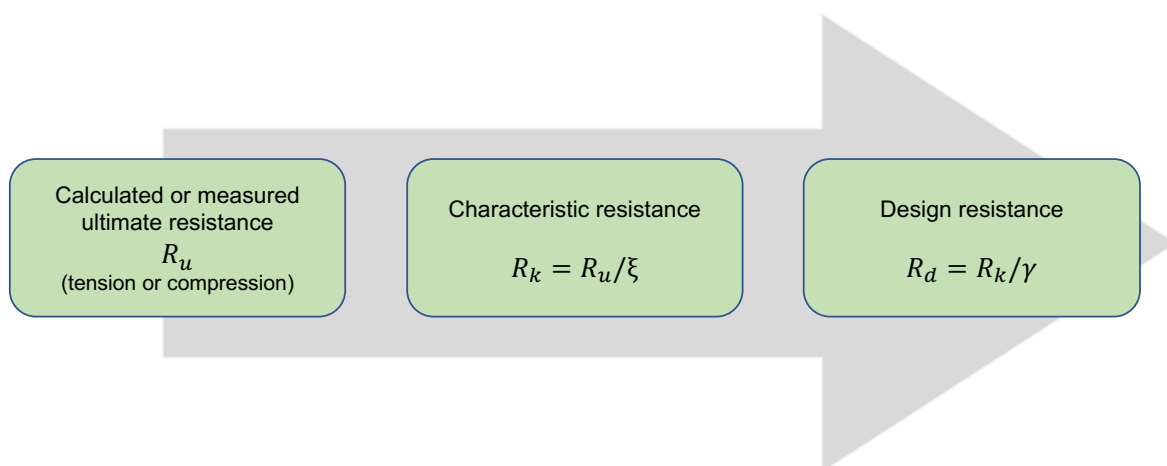


Figure 9 - EN 1997-1 three-step process to determine the pile design resistance

Where:

R_u is the axial ultimate resistance (either in tension or in compression);

R_k is the characteristic pile resistance;

ξ is a correlation factor suggested in EN 1997-1;

R_d is the pile design resistance;

γ is the partial safety factor.

2.3.2 Monotonic load-displacement behaviour

After understanding the static load resistance of piles, it is important to describe the load-displacement behaviour and the different moments of soil yielding and failure, as it depends on the relative mobilisation of the base and shaft resistances. As beforementioned, it is relevant to understand when and how the mobilisation of these two types of capacities take place, and, for the sake of analysing it, a load-displacement curve shape is sketched in Figure 10.

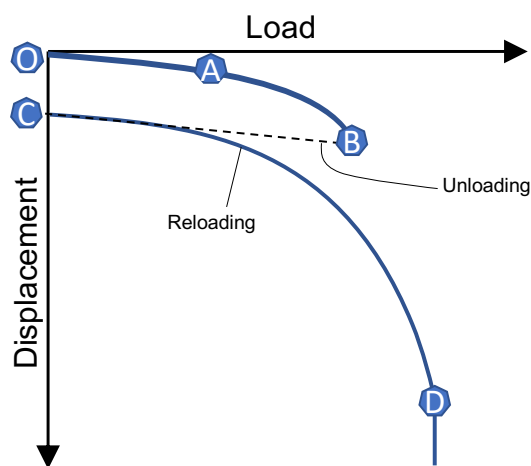


Figure 10 - Load-Displacement curve for compressive load to failure on pile, adapted from Tomlinson & Woodward (2008)

Figure 10 represents a pile being subjected to a progressively increasing compressive load, unloaded, and reloaded again. The different moments are identified by letters O, A, B, C and D, and are summarised by the following sequence (Tomlinson & Woodward, 2008):

O → A: Initially, the pile-soil system behaves elastically. The straight-line between points O and A, reflects the elastic behaviour in which, if the load is released at any stage up to point A, the pile head rebounds to its original position.

A → B: Beyond point A, the pile-soil system behaves plastically, meaning that yielding takes place and the load and displacement increase until point B is reached. Point B reflects the moment when the maximum shaft capacity will have been mobilised.

B → C: Since the plastic domain has been attained, if the pile is unloaded, it rebounds to point C, accumulating the permanent displacement OC.

C → D: When point D is reached, the full mobilisation of the base resistance is reached as well. Failure takes place and, consequently, the pile plunges downwards at a constant load, but increasingly large settlements.

The idealised load-displacement curve, as well as the moments where the resistances are mobilised, can be simplified by the representation on Figure 11.

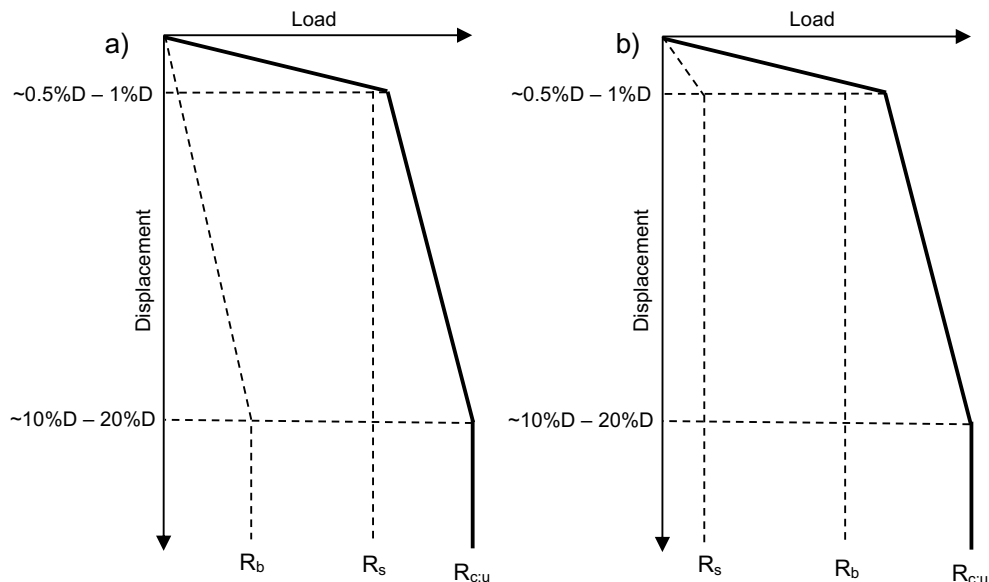


Figure 11 - Simple representation of the mobilisation of the resistances on a Load-Displacement curve for (a) replacement piles and (b) displacement piles

Figure 11 reflects a pile being subjected to a progressively increasing compressive load. It is visible that the displacement required to mobilise the maximum shaft capacity, R_s , is quite small, around 0.5% to 1% of the pile diameter, in both replacement and displacement piles. The base capacity, R_b , on the other hand, may require a greater displacement for its full mobilisation, in the range of 10% to 20% of the pile diameter. Since the level of confining stresses is higher in displacement piles (due to its construction method), the base capacity might be mobilised in the same range of displacements, Figure 11.b). Only once the pile shaft capacity has been fully mobilised, the 'stiffness' of the pile-soil system reduces to that of the pile base, and the displacements start to increase rapidly, leading to failure.

3 PILES UNDER AXIAL CYCLIC LOADING

3.1 GENERAL CONTEXT

Piles are often subjected not only to monotonic static loading, but also to cyclic axial loads and many studies examining the behaviour of piles under axial cyclic loading have been developed throughout the years, to scrutinize how this kind of load affects the stability of piles.

The term *cyclic* loading is defined as a repetitive and regular type of loading that follows a certain pattern, where variables such as amplitude, period and frequency can be easily determined by analysing the behaviour of the source of the cyclic loading (Andersen et al., 2013). Traditionally, the focus has been on offshore structures, with cyclic loading being imposed by natural influences i.e., wind, waves and earthquakes that correspond to relatively small periods, varying from as short as 1-second to as long as 10^2 -seconds. The periods and numbers of cycles characterising typical cyclic events are shown in Figure 12, where the shaded region located in the bottom-left corner indicates the domain of existing knowledge, while the range of the unshaded area suggests that little has been done to address longer loading periods and very large numbers of cycles.

One of the aims of this study is to explore the overall cyclic pile-soil behaviour when longer periods, compatible with cyclic thermal loading of energy piles (i.e. months to years), and limited numbers of cycles ($N < 50$ where N represents e.g. 1 annual cycle) are considered.

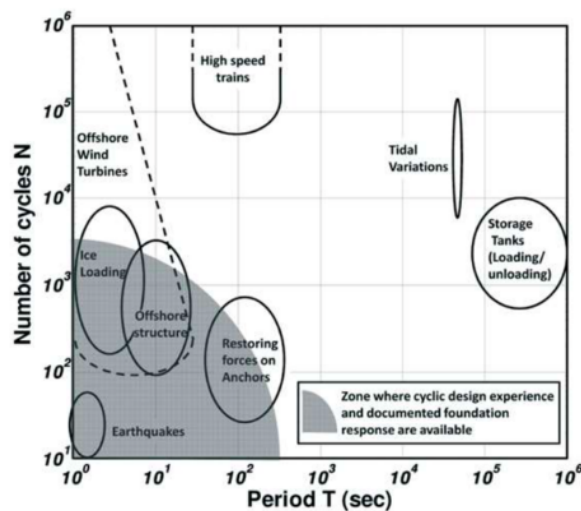


Figure 12 - Periods and number of cycles of typical cyclic loading events, Andersen et al. (2013)

Up until the 1970s, the design of offshore foundations was based on the peak static load, nonetheless, the real loading to which they are subjected is far more severe than this. As

experience of offshore foundation performance evolved, cyclic effects became a critical phenomenon to take into consideration when designing these type of structures (DeJong et al. 2003).

In this Chapter, the effect of cyclic axial loading on the stability of piles is reviewed, placing particular emphasis on variables such as the installation method, cyclic and ultimate load, number of cycles and their effects on the ultimate resistance and load-displacement behaviour of piles, as well as potential changes in soil stresses.

3.2 CHARACTERISATION OF CYCLIC LOADS

In real-world scenarios, cyclic loading is non-regular, meaning the amplitude and/or period of loading are irregular, making it difficult to characterise it by means of regular, periodic functions such as that illustrated in Figure 13. However, such simplifications are made to facilitate analysis as well as to undertake experimental testing.

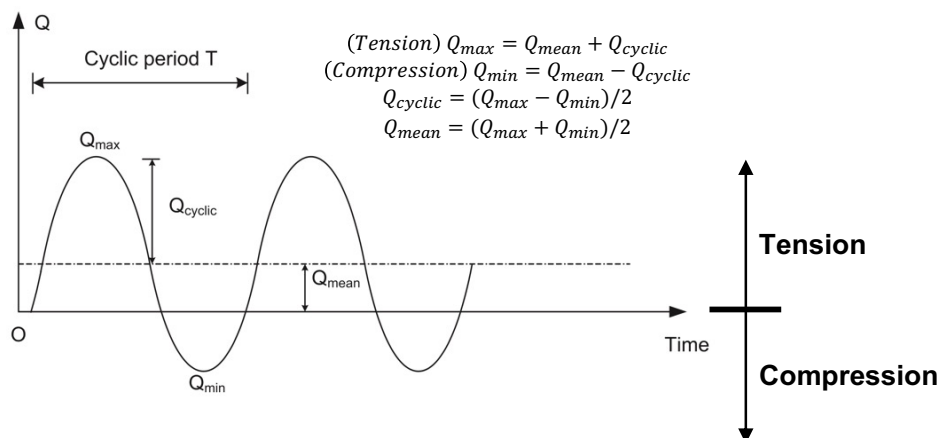


Figure 13 - Cyclic axial loading variables, Jardine & Standing (2012)

Consequently, it is necessary to define certain parameters to indicate a range of cyclic values. The cyclic load parameter Q_{mean} is the mean load or mean component of the cyclic load, while Q_{cyclic} is the axial cyclic load amplitude increment or half-amplitude of the cyclic load, providing the peak cyclic loads Q_{max} and Q_{min} . T is the period of the cycles (thus $f = 1/T$ corresponds to the frequency) and lastly, N is the number of cycles applied.

In pile behaviour studies, cyclic loading is classically distinguished between *one-way* and *two-way* loads as follows:

- *one-way* load tests, either in tension or compression, where $Q_{cyclic} < Q_{mean}$;
- *two-way* load tests, alternating tension-compression, where $Q_{cyclic} > Q_{mean}$.

Cyclic loading can have a significant influence on the behaviour and stability of foundations during their lifetime and cause, in the medium and long term, significant pathologies and disorders that can go as far as major dysfunctions that endanger the structure, hence the importance of this study.

3.3 CONCEPT OF CYCLIC STABILITY DIAGRAM

Poulos (1988) described the effect of cyclic loading through a cyclic stability diagram where the results were presented in terms of the ratio $Q_{cyclic}/Q_{ult,t}$ as a function of $Q_{mean}/Q_{ult,t}$, for a fixed number of load cycles, N , as shown in Figure 14. Where Q_{cyclic} and Q_{mean} were defined in Figure 14, $Q_{ult,c}$ is the ultimate monotonic compression resistance $Q_{ult,t}$ is the ultimate monotonic tension resistance (pull-out capacity). Such a normalised representation allows the results from various studies under the same conditions to be compared.

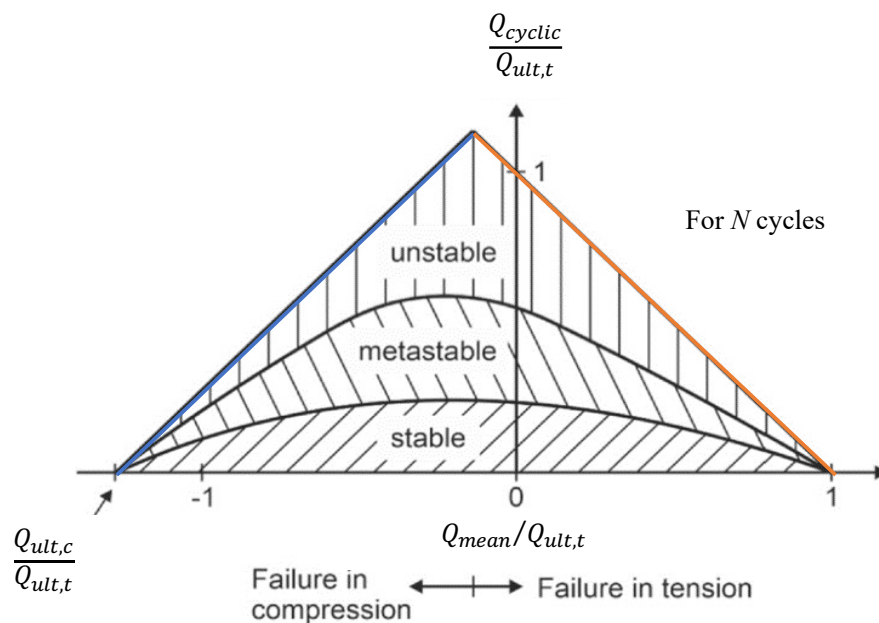


Figure 14 - Cyclic Stability Diagram, Poulos (1988)

The definition of *failure* under cyclic loading refers to the development of a limiting accumulated displacement. For the design of offshore structures, it is considered that failure takes place when a displacement equal to 10% of the pile diameter, D , is attained (Puech & Garnier, 2017). Within the diagram, three behaviour categories are defined: *stable*, *unstable* and *metastable*:

- The *stable* zone as the one in which only small deformation accumulation might occur without occurring failure;
- The *unstable* zone, where cyclic loading will result in failure of the pile within a specified number of cycles;
- The *metastable* zone lies between the *stable* and *unstable* zones and, in this zone, cyclic

loading causes a limited accumulation of deformation, leading ultimately to failure.

The diagram developed by Poulos (1988) considers a two-way cyclic load, hence the pile response can be either in compression or in tension. The diagram is then asymmetrical in relation to the vertical axis because the compressive capacity is usually greater than the tension capacity, as the base resistance is mobilised in addition to the shaft.

In Figure 14, the coloured lines represent failure in tension (orange) or compression (blue) under monotonic loading (combinations of $Q_{\text{mean}}/Q_{\text{ult,t}} + Q_{\text{cyclic}}/Q_{\text{ult,t}} = 1$), whilst the internal boundaries correspond to the load ratios that lead to a change in the stability zone. As N increases, the *stable* and *metastable* zone boundaries will tend to shrink, with the cyclically *unstable* zone increasing in size. It should be expected that different stability diagrams apply for different pile types, pile dimensions, and soil conditions, even though it is not yet fully understood how all these parameters affect the pile behaviour under cyclic axial loading (Achmus et al., 2020).

3.4 EFFECTS OF CYCLIC AXIAL LOADING AND INFLUENCING FACTORS

Most offshore structures are likely to experience thousands to, potentially, millions of load cycles with variable magnitudes, frequencies, and other load components during their service lives. Hence, a broad range of foundation types may be considered for these offshore projects, including monopiles, gravity base structures, although the most commonly used are driven piles (Gavin et al., 2011).

Pile driving during installation creates displacement of the surrounding ground and alters various soil properties. During the process of installation, as the pile is driven into position, many cycles of shearing take place, that is, the soil around the pile is disturbed by the continuous movement and the strength is weakened (Li, 2019). This is directly linked to particle breakage next to the pile shaft, as well as at the pile base, which implies that a loss of the shaft resistance with respect to undisturbed soil conditions has already occurred, even before any cyclic axial loading is applied. Therefore, these effects must be considered, when studying and designing driven piles.

Having said this, the response of soils to cyclic stresses is complex and numerous phenomena are linked with the effect of cycles, namely (Puech & Garnier, 2017):

- The degradation of the shaft resistance over many cycles, which reduces the bearing capacity. Long-term uncontrollable displacements may take place;
- The generation of excess pore pressures, which reduces the effective stresses and can lead to the phenomenon of liquefaction.

3.4.1 Degradation of the shaft resistance

One of the most relevant factors to take into account is the degradation of shaft resistance. Real-world piles are relatively compressible, and soils exhibit mechanical properties which improve with depth, so the phenomenon of cyclic degradation with depth is crucial to understand and evaluate the overall response of a soil-pile system. It follows naturally from this that any loss of capacity on the pile shaft must be compensated by the transfer of loads to the other parts of the shaft and the base of the pile. Cycle by cycle, friction degradation tends to propagate along the shaft from the head, towards the base of the pile.

Experimental tests made by Poulos (1991) and later cited by Andersen et al. (2013), showed that pile foundations under cyclic loading have a smaller shaft capacity when compared to that of monotonic loading, as shown in Figure 15. Thus, as the number of cycles N increases, the shaft capacity tends to decrease.

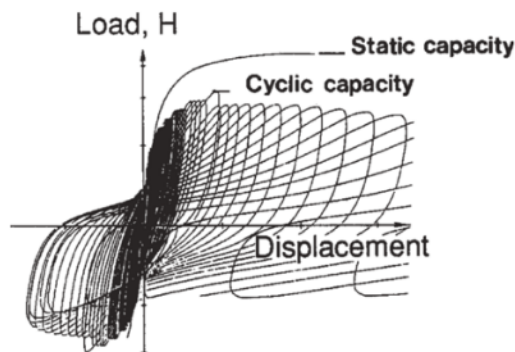


Figure 15 - Results from model tests with monotonic and cyclic loading, Poulos (1991)

To understand the phenomena of the degradation of shaft resistance, one must first conceptualise what occurs in the pile-soil interface zone. Fioravante (2002) explains the interface behaviour between the pile shaft and soil by the conceptual model shown in Figure 16.

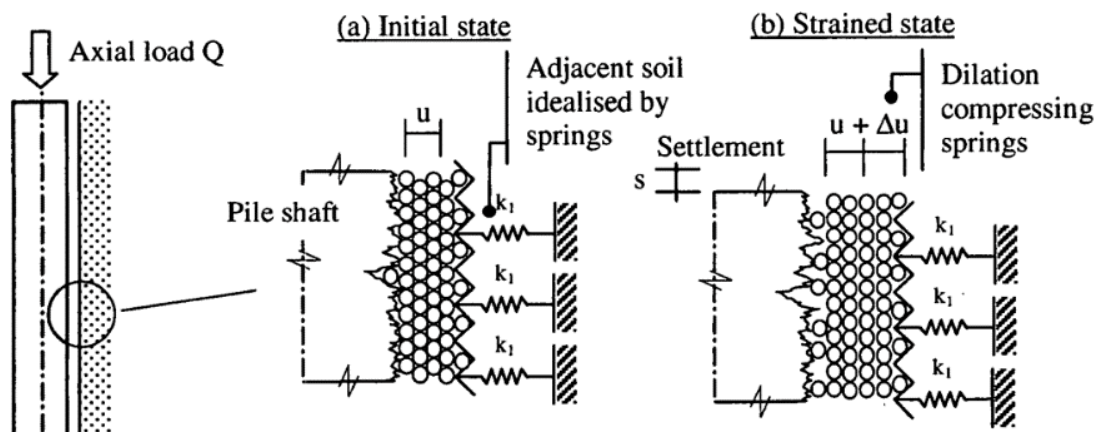


Figure 16 - Conceptual Model of pile-soil interface friction, Fioravante (2002)

In this conceptual model, the author describes that, in the interface between the pile shaft and the surrounding soil, any volume change in this zone is constrained by the surrounding soil, acting as an “elastic spring”. In other words, the tendency of the interface layer to change its volume interacts with the behaviour of the surrounding soil, which imposes the normal stiffness condition on the interface between the pile and soil. Thus, the normal effective stress to the pile-soil interface, σ'_n , can increase or decrease when soil exhibits dilative or contractive behaviour, respectively. According to Fioravante (2002), experimental evidence shows that the increment of the normal effective stress, $\Delta\sigma'_n$, can be estimated through the Eq. 3.1.

In the “elastic spring” conceptual model, Fioravante (2002) rationalises the skin friction mechanism along the pile shaft through a simple model test named the “Interface Direct Shear Test” with constant normal stiffness, k_1 , shown in Figure 16. It consists of a rigid plate with a specified roughness, simulating pile shaft, sliding against a soil specimen that is confined in a direct shear apparatus and subjected to a variable normal stress, σ'_n . As the soil tends to dilate ($\Delta u > 0$) the normal applied stress increases ($\Delta\sigma'_n > 0$) and vice versa, as this allows the normal stiffness applied to keep constant, defined in Eq. 3.2.

$$\Delta\sigma'_n = \frac{2G}{R} \Delta u \quad (3.1)$$

$$k_1 = \frac{\Delta\sigma'_n}{\Delta u} \quad (3.2)$$

Where:

$\Delta\sigma'_n$ is the increment of the normal effective stress;

G is the strain and pressure dependent shear modulus of soil;

k_1 is the “elastic spring” stiffness

R is the pile radius;

Δu is the displacement normal to the pile shaft of soil in the interface zone.

Patel (2011) reviewed the hypothesised friction fatigue mechanism (also known as shaft resistance degradation) proposed by White and Bolton (2002), Figure 17. The author acknowledges that a similar mechanism can be expected for reduction of pile capacity under cyclic loading. The reduction of horizontal effective stress acting on the pile shaft is governed by two processes:

Process 1- Volume reduction in Zone B due to continued shearing at the pile-soil interface:

It is hypothesised that this process is associated with two mechanisms of volume reduction. Firstly, rearrangement and repacking of the sand grains is caused by mixing at the rough pile surface. Secondly, further repacking in the boundary layer is permitted by diffusion of fine

broken particles away from the pile-soil interface into the more open matrix of uncrushed soil in the far field.

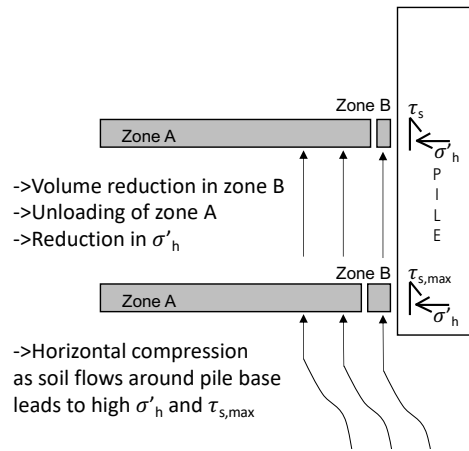


Figure 17 - Friction Fatigue mechanism proposed by White and Bolton (2002)

Process 2- Horizontal unloading in Zone A:

This is a continuum unloading process. Zone A can be represented as a spring with the governing stiffness which would depend on the *in-situ* soil properties and installation-induced stress and strain level.

As a consequence of the friction fatigue, it is pertinent to consider the accumulation of permanent displacement with the increasing load cycles N . Andersen et al. (2013) confirmed that, when comparing static with cyclic loading, the latter tends to develop large permanent displacements with lower levels of mean loading, Q_{mean} , applied.

When cyclically loaded, the particles of soil surrounding the pile will crush and consequent degradation of shaft (Chapter 3.4.1) and base resistance take place, leading to soil fatigue. This is understandably the same reason for higher accumulation of permanent displacement, since particle crushing will allow particle rearrangement and, subsequently, the pile will have the freedom to relocate little by little until reaching failure, Figure 18.

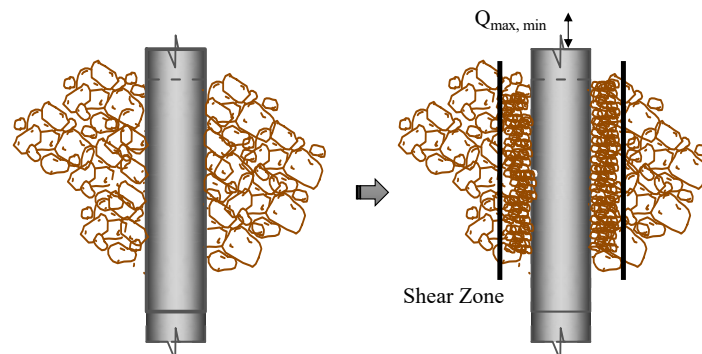


Figure 18 - Particles tendency to crush when submitted to cyclic loading

3.4.2 Influence of installation method

As reported by Poulos (1991), the installation methods described in Chapter 2.2 have an influence on the cyclic response of a pile, where displacement piles generally have a stiffer cyclic response than replacement piles. During the displacement piles installation, there is an increase in confining stress and stiffness of the soil adjacent to the pile and, as consequence, more permanent displacement on replacement piles is expected rather than on displacement. Mainly because, during installation, displacement piles have already undergone greater plastic deformations at the base (Li et al., 2012).

Although, generally speaking, cyclic loads lead to degradation of the shaft resistance and increased deformation (Jardine & Standing, 2012), it has also been shown that this kind of load can indeed improve the bearing capacity, as long as only a small number of fast cycles are applied, allowing creep, drainage and rearrangement of particles without crushing them (Andersen et al., 2013). Thus, if the rate of cyclic loading is relatively high, the rate effects will tend to counteract the degradation. It is generally assumed however that the base resistance is almost unaffected, meaning that the degradation only compromises the shaft resistance capacity.

3.5 DESIGN OF CYCLICALLY AXIALLY LOADED PILES

Bearing in mind the previously mentioned, it is logical to admit that, when designing a pile submitted to cyclic axial loading, the following verifications/failure possibilities need to be examined:

- 1- Cyclic effects on the pile capacity;
- 2- Number of cycles N that the pile can withstand before failure;
- 3- How acceptable the accumulated displacement is.

In the European regulations, *Eurocode 7 – Part 1* (EN 1997-1:2004) it is affirmed that the *severe adverse effect of cyclic loading and reversals of load on the tensile resistance shall be considered* (§7.6.3.1), it is not clear how to take into account these effects, as there are no generalised calculation methods (Achmus et al., 2020). Nevertheless, a common task is to assess whether the pile can withstand the equivalent load cycles derived for a certain cyclic reference load, *i.e.* whether the number of load cycles is sufficiently below the number of load cycles leading to failure, hence checking safety. Another approach commonly used is to consider a reduced bearing capacity, for instance, taking 40% of the ultimate static bearing design capacity (Achmus et al., 2020). Or even, consider a maximum acceptable displacement as 10% of the pile diameter. Evidently, in all approaches the expected displacement needs to

be addressed. Various approaches concerning the design of these piles are thoroughly explored in e.g., Puech & Garnier (2017). This is not, however, the goal of this study.

3.6 FULL-SCALE CYCLIC AXIAL LOAD TESTING OF PILES

Although there is a vast number of experimental literature of small-scale and full-scale cyclically and axially loaded piles, the process of reviewing and creating a database of the existing tests on pile foundations, for the present dissertation, has proven to be quite challenging. It has been found that the parameters involved in the tests vary from article to article e.g., most do not mention the period/frequency of the cyclic load – one of the key factors influencing the cyclically loaded piles; the soil initial state nor its properties; providing either relative or absolute of Q_{mean} and Q_{ult} ; varying failure criteria, among others. Hence, it complicates the comparison between tests and the development of a consistent framework for describing cyclic axial loading effects on piles. For this reason, a very limited number of experimental tests are analysed in this Chapter.

In the framework of the French project SOLCYP (Puech & Garnier, 2017), the axial cyclic loading effects in piles were investigated in-depth. Small-scale model piles and full-scale prototype piles were tested and in the following they are described and conclusions about their performances summarised.

The test method was uniformised across the project, thus:

- 1) The pile was tested statically in tension and/or in compression, to obtain the reference values for $Q_{\text{ult,t}}$ and $Q_{\text{ult,c}}$, respectively.
- 2) Depending on the goal of the particular study, apply different combinations of cyclic loading with a period T , or frequency f , until reaching failure after the number of cycles N_f .
- 3) In all tests, failure was considered to be reached when displacements at the pile head were equal to $10\%D$.

3.6.1 Plancoët, near St. Malo, France

The first full-scale cyclic axial load tests ever conducted were by the *Institut Français du Pétrole* in Plancoët, Brittany, France in 1978. A driven close-ended metallic pile with a diameter $D = 273$ mm and length $L = 13$ m was installed in a soil profile comprising silts and loose sands. No indications about the ground water level are provided. The pile was subjected to up to 1500 cycles of *one-way* tension loading ($Q_{\text{max}} = Q_{\text{cyc}}$; $Q_{\text{mean}} = 0$) with load ratios of $\frac{Q_{\text{max}}}{Q_{\text{ult,t}}} = 0.40$ (global factor of safety, $FS = 2.5$) and for $\frac{Q_{\text{max}}}{Q_{\text{ult,t}}} = 0.25$ ($FS = 4.0$). The results obtained are illustrated in

Figure 19, which shows the pile head displacements z [mm] versus the number of load cycles N , applied with a period, $T = 14$ s ($f = 0.07$ Hz).

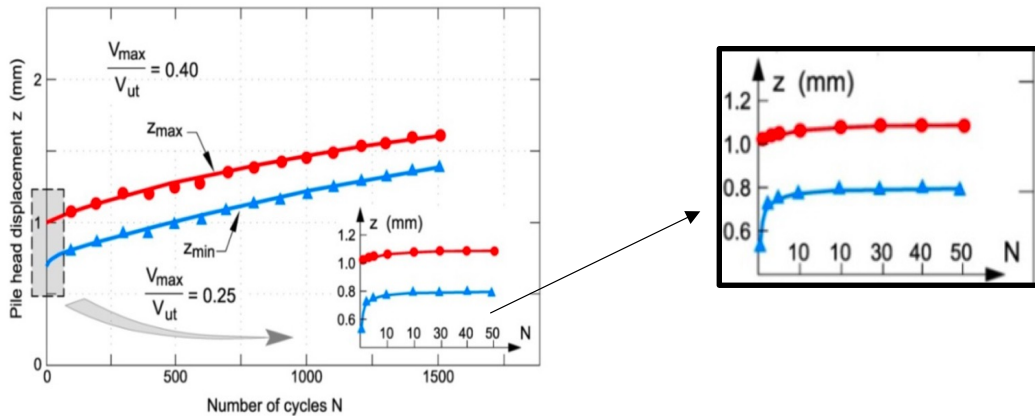


Figure 19 - Pile head displacements(z)-Number of cycles (N) curve, Puech & Jezequel (1981)

In both $\frac{Q_{max}}{Q_{ult,t}}$ combinations ($\frac{V_{max}}{V_{u,t}}$ in Figure 19), the pile head displacement accumulated rapidly in the first 50 cycles and the subsequent displacement rate seems to stabilise, as the number of cycles accumulates to hundreds, the displacement continues to accumulate throughout the test. This suggests that, even after hundreds of cycles, no stabilisation of pile top displacements has occurred, in spite of large FS values with respect to the ultimate tension resistance.

As N increases, the displacement response accumulates to about 0.6 mm (0.20%D) for $\frac{Q_{max}}{Q_{ult,t}} = 0.40$ and 0.9 mm (0.33%D) for $\frac{Q_{max}}{Q_{ult,t}} = 0.25$, which is far from the failure criteria of 10%D.

It is then possible to relate this fact with the concept of the Cyclic Stability Diagram mentioned in Chapter 2.3: the merely apparent stabilization at $N = 50$ cycles corresponds to the narrow *stable* zone, leading to a large *metastable* zone, sketched in Figure 20.

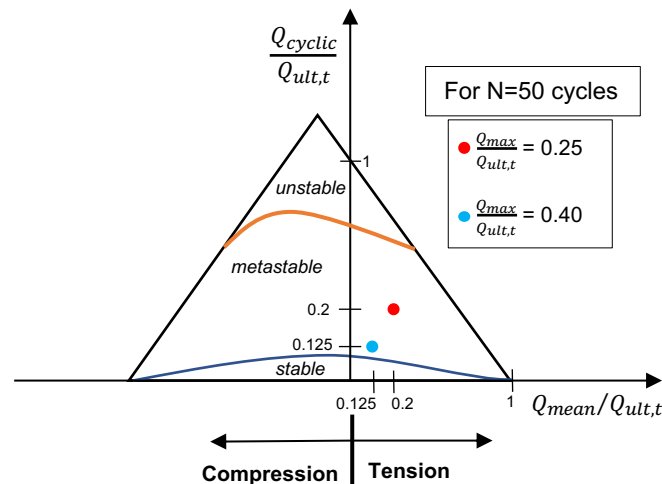


Figure 20 – Sketch of Cyclic Stability Diagram based on Puech & Jezequel (1981) results

3.6.2 Loon-Plage, near Dunkirk, France,

In this study, two *one-way* cyclic tests were carried out: one in tension (Q_{max}) and another in compression (Q_{min}) in dense to very dense sands in Dunkirk, France, Benzaria et al. (2013).

The tested piles, with diameter $D = 420$ mm and length $L = 8$ m, were CFA piles and the different load combinations tested were: $Q_{max}/Q_{ult,t} = 0.63$ (FS = 1.6), and $Q_{min}/Q_{ult,c} = 0.32$ (FS = 3.1) with a period $T = 2$ s, Puech & Garnier (2017). The respective number of cycles to failure N_f are summarised in Table 2.

Table 2 - Test results, by Benzaria et al. (2013)

Test #	$Q_{max}/Q_{ult,t}$	$Q_{min}/Q_{ult,c}$	$Q_{mean}/Q_{ult,c/t}$	N_f
1	0.63	-	0.32	367
2	-	0.32	0.16	>2000

3.7 SMALL-SCALE CYCLIC AXIAL LOAD TESTING OF PILES

3.7.1 Small-scale testing fundamentals

The testing of full-scale geotechnical structures, such as piles, is relatively difficult and expensive compared to small-scale testing. However, provided that similitude rules are respected, small-scale testing can provide a good representation of the prototype (full-scale) structure. Such rules have been developed and improved by many authors, for small-scale testing under the action of either 1 gravity, 1g, or in the centrifuge, with $> 1g$ conditions.

Physical modelling makes it possible to study the problem of foundations in three dimensions, taking into account the non-linear behaviour of soil. The model cannot exactly reproduce all the characteristics of the full-scale structure, but it makes it possible to duplicate the tests in order to verify an observation, to carry out parametric studies, to benefit from the ideal conditions for reconstruction and implementation, and to carry out the tests until failure (Blanc et al., 2015).

A catalogue identifying similarity rules for application in small-scale geotechnical testing was published by Garnier et al. (2007). The main relationships useful for the present study are summarised in Table 3 where N_a denotes the intensity of the acceleration to which the model is subjected (model factor).

From the similarity conditions detailed in Garnier et al. (2007), the list of scale factors can be drawn up which allow the results of the tests in scale models to be converted into prototype sizes through Table 3.

Table 3 - Scaling factors for different parameters

Variables	Scaling Factor (Full-scale to Small-scale)
Acceleration	1
Length and displacement	$1/ N_a$
Strain	1
Force	$1/ N_a^2$
Stress	$1/ N_a$
Mass	$1/ N_a^3$
Weight	$1/ N_a^3$
Time	1

3.7.2 Blanc et al. (2015)

Blanc et al., (2015) consider a prototype pile with a diameter, $D = 1.8$ m, and length, $L = 40$ m, which based on a model factor of 100, yields a small-scale model with 1.8 cm of diameter and 40 cm of length. The goal is to replicate a driven pile, after the soil is put in place, a small hydraulic jack was installed at the pile head to induce load, along with a load cell to record it.

In the study, both *one-way* (tension only) and *two-way* loading tests on six piles in a dense Fontainebleau sand NE34 were undertaken in a centrifuge, at an acceleration of 100-*gravities*, to determine the number of load cycles, N_f that lead to failure at differing load ratios and a constant period, $T = 10$ s, with the results summarised in Table 4.

Table 4 - Small-scale test results, Blanc et al. (2015)

Test #	One/Two-way	$Q_{max}/Q_{ult,t}$	$Q_{min}/Q_{ult,c}$	$Q_{mean}/Q_{ult,c/t}$	N_f
1	One-way	0.84	-	0.42	230
2	One-way	0.56	-	0.28	>1500
3	One-way	0.93	-	0.47	133
4	Two-way	0.05	0.06	0.05	>1500
5	Two-way	0.22	0.32	0.27	>1500
6	Two-way	0.36	0.51	0.43	33

It is then shown that failure in compression is reached for higher values of Q/Q_{ult} and N_f than for those of tension. This is related to the fact that in tension, there is only one type of mobilised resistance, the shaft, while in compression there is also the resistance mobilised at the base. This fact is reflected on the Cyclic Stability Diagram, shown in Figure 21, by having a larger area for Q_c than for Q_t . Note that, in this experimental campaign, the author opted for a contrary convention of the Cyclic Stability Diagram, by considering the failure in compression in the positive x-axis.

From the results shown in Table 4, two-way loading tests can be more severe in terms of failure, since in the tests #1, #3 and #6 for similar values of mean normalised load, $Q_{mean}/Q_{ult,c/t}$, the number of cycles leading to failure are higher in the one-way tests.

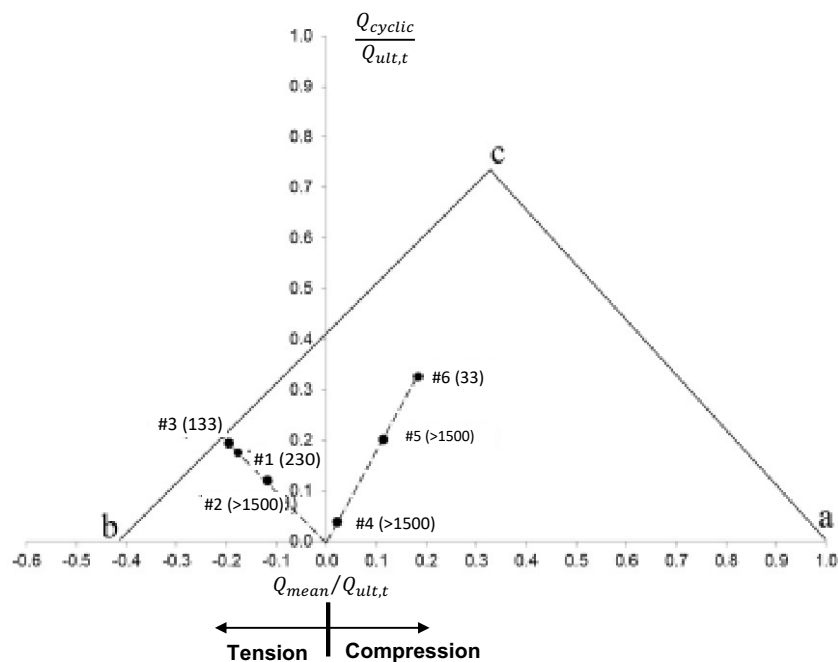


Figure 21 - Cyclic Stability Diagram, adapted from Blanc et al. (2015)

3.8 SUMMARY OF EXPERIMENTAL CASE STUDIES

It is now fundamental to understand what the worst-case scenario is, in other words, which combination(s) of loading, number of cycles and loading period are the most likely to lead to failure. In Table 5 all the aforementioned parameters are organized, with increasing Q/Q_{ult} ratios.

After careful examination of Table 5, it is evident that the main factors contributing to failure are the loading applied, as well as its frequency, since for higher values of Q/Q_{ult} and higher frequencies, failure tends to take place at lower levels of N_f . On the other hand, the soil density little modifies the bearing capacity, once for similar values of load ratio and frequency, but opposite soil density conditions, N_f remains unchanged. Logically speaking, a dense sand will have a higher static resistance when compared to a loose sand and, therefore, for any given load ratio, a larger load cycles take place. Nonetheless, it may be that, for cyclic loading, the effect of initial state of the soil is not so important, as it is altered from cycle to cycle.

Table 5 - Summary table of experimental literature review

Reference	Soil	$Q_{mean}/Q_{ult,t}$	$Q_{max}/Q_{ult,t}$	$Q_{min}/Q_{ult,c}$	f [Hz]	N_f
Blanc et al. (2015)	Dense sand	0.06	0.05	0.06	0.10	>1500
Puech & Jezequel (1981)	Loose sand	0.13	0.25	-	0.07	
Blanc et al. (2015)	Dense sand	0.27	0.22	0.32	0.10	
Puech & Jezequel (1981)	Loose sand	0.20	0.40	-	0.07	
Blanc et al. (2015)	Dense sand	0.44	0.36	0.51	0.10	33
Benzaria et al. (2013)		0.32	0.63	-	0.5	367
		0.16	-	0.32		>1500
Blanc et al. (2015)		0.28	0.56	-	0.10	230
		0.42	0.84	-		
		0.47	0.93	-		

4 MATERIALS AND METHODS

In order to achieve the objectives of this thesis, a series of tests were conducted on a single pile at the geotechnics laboratory of Instituto Superior Técnico, University of Lisbon. The goal of this experimental campaign was to simulate, through a small-scale model, the behaviour of a single pile installed on sand, under cyclic axial loading. The tests were run under controlled conditions, so these would remain constant throughout the experimental tests and this Chapter details the materials used and methods developed to achieve this. A brief checklist describing how to setup and run a test was created and is presented in Appendix A.

4.1 EQUIPMENT

The testing setup is rather simple, in fact, it is similar to various experimental setups described in the literature, e.g. Li et al. (2012). The materials and equipment consisted of (Figure 22): a steel loading frame (repurposed from an existing consolidation frame), a large steel tank, a sandy soil, a small-scale aluminium pile, a linear stepper motor, a 1000 N load cell, a displacement transducer (POPT), a data logger, a computer with the data acquisition system and motor control software installed, and a large wooden storage box for holding the sand.

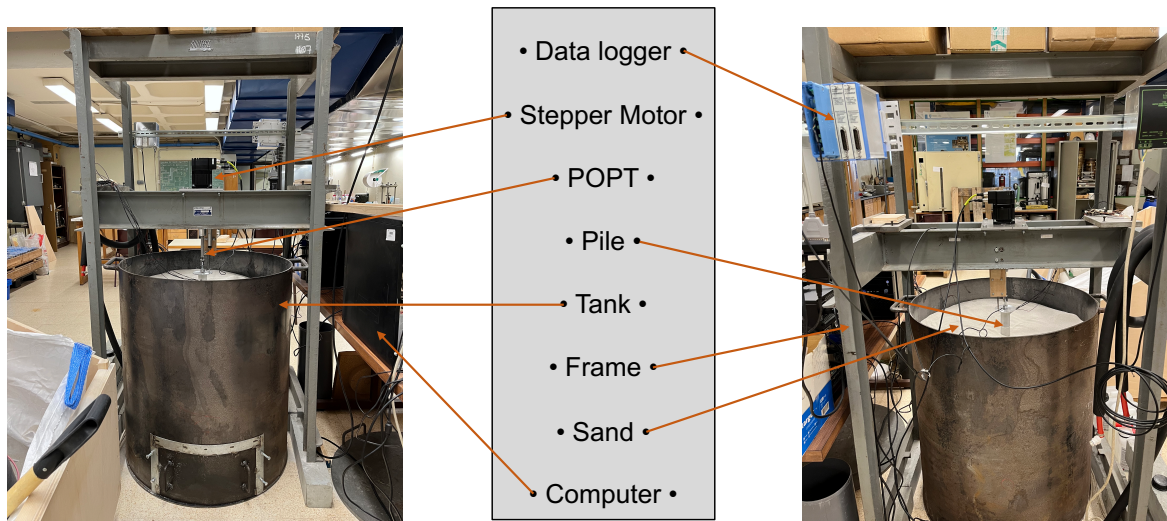


Figure 22 - Laboratory Test Setup

4.1.1 Small-scale model pile

There could be no *Small-scale model testing of cyclically axially loaded piles* without the main ingredient – the pile. The model pile was fabricated from an AS-6063 aluminium tube with an outside diameter of 40 mm and wall thickness of 5 mm, Figure 23. The model pile has

a total length of 760 mm (weighing 1.17 kg), of which 600 mm is embedded in soil for the tests, and its schematic view with dimensions is present in Appendix B.

The model pile was fabricated in six parts which screw together to complete the pile body; this was to allow the placement of axial strain gauges along the inside surface of the pile but also allows modifications to the pile geometry to be made. The aluminium tube is smooth finished and during fabrication a knurled finish was imprinted on the completed parts to increase the surface roughness. Five of the parts represent the pile body while the last makes up the pile head. In this part, provision has been made to allow any internal sensor cables to exit the pile, a 100 mm diameter aluminium ring can be attached, to provide a landing surface for the displacement transducer), and to provide a threaded connection point for attaching the load cell.

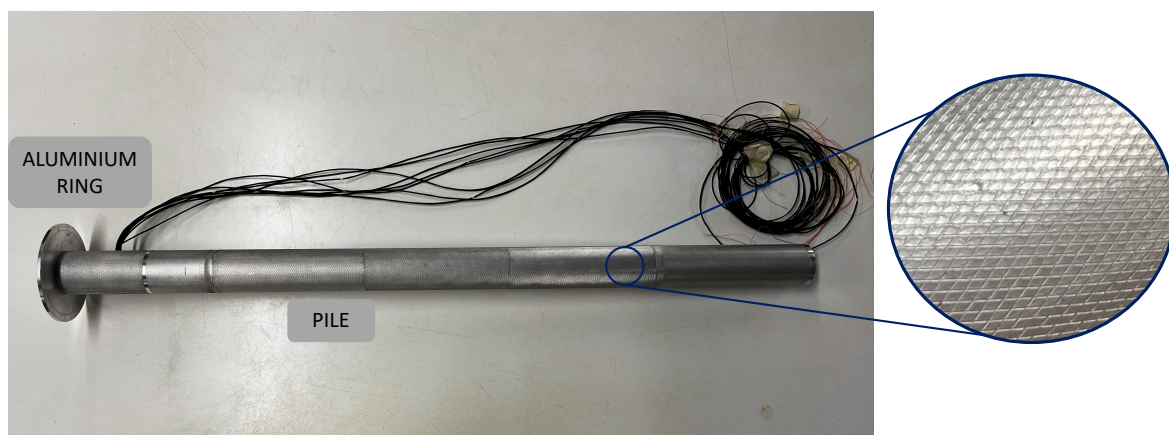


Figure 23 - Small scale Pile and its texture

Note that in Figure 23, the cables exiting near the pile head are from axial strain gauges glued along the inside of the model pile. These have not been used in the tests made to-date and are not discussed further.

4.1.2 Stepper Motor

Often, pile tests are run as load-controlled, i.e. an increment of force is applied and the pile settlement response measured but they can also be displacement-controlled with the pile reaction resulting from an increment of vertical displacement being measured. In the planned tests, it was decided that displacement-control would be employed: a) because thermal loading is a strain-imposed effect on the pile and b) it was felt that it would allow for better control of load cycles.

Stepper Motors are well suited for applications which require precise position control. The motor used in this experimental campaign was a 24V MIL34 stepper motor linear actuator sourced from *JVL – Industri Elektronik* (serial no. 212822) which has rated axial thrust of

2000 N. The motor was supplied with a 150 mm lead screw (118 mm travel) with a thread pitch that provided 5.08 mm (0.2") travel per revolution, an integrated electronic controller unit and a displacement encoder. In this motor, the rotational motion of the stepper motor is translated to a linear translation, along the axis of the lead screw, via a specially fabricated plastic nut.

The translation imposed on the plastic nut is very finely controlled as the motor resolution is 409600 steps per revolution, i.e. 1 step equates to 1.24×10^{-5} mm travel of the nut, and some reference values used in the testing are shown in Table 6. In the control software, the required number of steps are programmed to give the desired displacement, along with the desired loading rate (revolutions per second), see Chapter 5.4. The main limitation of the motor is its rated thrust of 2000 N, however the pile ultimate compression resistance is expected to be less than 1000 N, which is the rating for the load cell (Chapter 5.1.4).

Table 6 - Reference values for the equivalence between required displacement a stepper motor steps (409600 steps per 5.08 mm)

Displacement [mm]	Number of steps
1	80 630
5	403 150
30	2 418 900

The role of the motor is to induce a certain amount of displacement at the pile head, to which it is attached as shown in Figure 24. The motor is fixed to an 8 mm aluminium plate which is in turn attached to the load reaction frame. The lead screw passes through a hole in the plate and a special adapter was fabricated, to provide a connection between the plastic nut and the load cell and model pile.

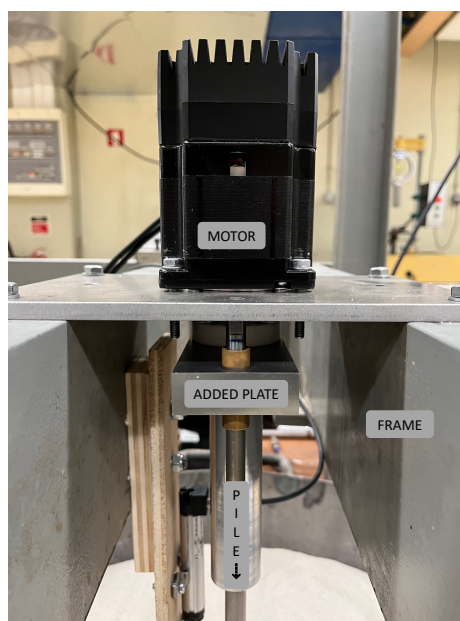


Figure 24 - Detail of Motor-Frame and Motor-Pile connection

In Figure 24, an “added plate” is indicated; during the initial tests described in Chapters 5.1 and 5.2, it was found that there was insufficient torque resistance in the system and the pile would rotate on the nut without translating. This was overcome in an ad hoc manner by holding the adapter, between the nut and the load cell, to allow the tests to proceed. Subsequently, a restraint system was added which consisted of the indicated plate plus two vertical bars which acted as guides and provided the torque restraint needed. One of the bars can be seen along with the (yellow) brass bushing that allows it to traverse the “added plate”.

4.1.3 Potentiometric Position Transducer (POPT)

The displacement transducer is a very precise sensor (resolution < 0.01 mm and linearity error of 0.1%) that can convert the linear motion of an object, to which it is coupled, into a corresponding electrical signal. In other words, it is used to measure the pile head vertical displacement, a key parameter in this experimental campaign. The POPT used was a *Novotechnik TEX-0050 series* sensor with a range of ± 25 mm. In the test setup it is fixed to the load frame and sits on a platform provided at the pile head, as indicated in Figure 25.b).

The model of POPT used has a return spring design that allows a measurement without a fixed connection to the moving part. Each test would start with it being compressed, so that: in compression tests (pushing downwards) the spring would ease/relax, and in tension tests (pulling upwards) the spring would be strained even further always measuring the increment of displacement achieved (Figure 25).

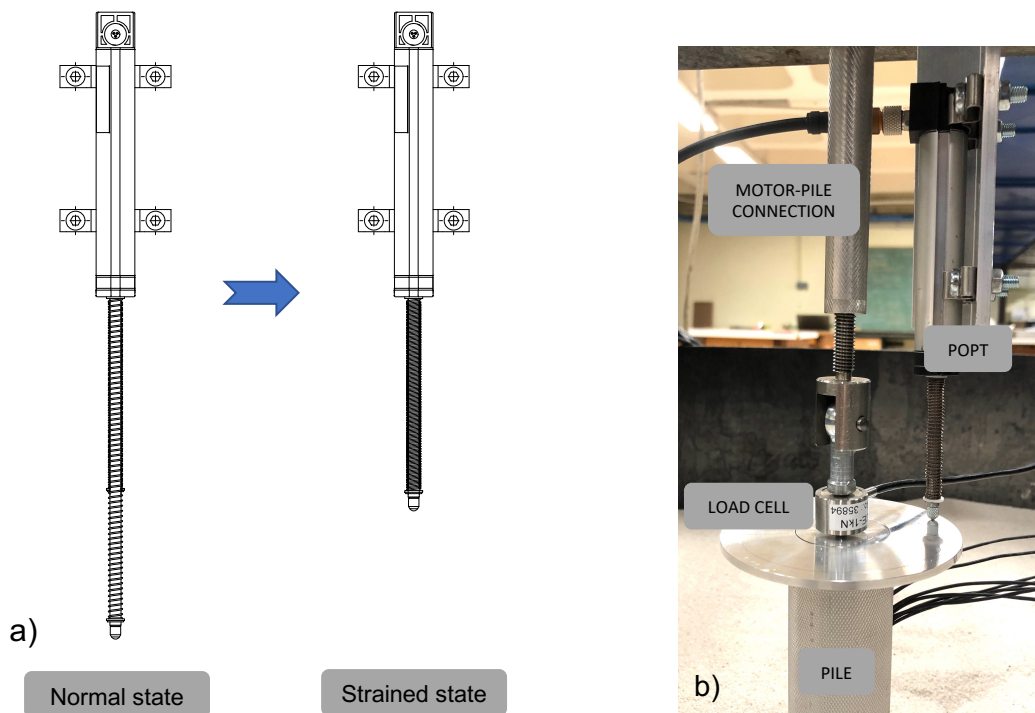


Figure 25 - POPT (a) return spring mechanism and (b) in place prior to test

By converting displacement into electrical signals, the displacement transducer communicates the data to the data logger, see Chapter 4.5. This data was recorded and provided confirmation that the specified/programmed stepper motor movement was as intended.

The POPT has a maximum range of displacement read of 50 mm. This implies that before running a test, one must carefully check how compressed the spring already is, e.g. if it is compressed 20 mm, this signifies that only a 30 mm increment is possible for tests in tension, or 20 mm in compression. This did not affect the tests, however, since the maximum displacement tested was 30 mm.

4.1.4 Load Cell

The load cell is a sensor that converts force into a corresponding electrical output signal which can be captured and recorded by the data logger. The miniature DCE 1 kN load cell used in this study was supplied by LCM Systems and was factory calibrated for measurements in tension and compression up to the rated load of ± 1000 N. It has a resolution of 1 N and exhibits non-linearity of $<0.25\%$ of the rated load (2.5 N). The 1 kN model was chosen as the maximum loads expected were less than this and it minimised the potential non-linearity in the measurements.

The load cell is screwed into the pile head and is attached to the motor-pile connection via a rod-end bearing that allows the connection to hang vertically, Figure 25.b).

4.1.5 Data Acquisition Hardware and Software (Data logger)

The data logger is an apparatus used to convert electrical signals into data, transmitting it to a computer in real-time. The data acquisition hardware used was supplied by *GW Instruments Inc.*, and it is a low-cost modular system with USB-based communications. The data logger used for this study comprises an iNet-555 starter kit, which includes an 8 channel iNet-430 card with an extra two iNet-420 expansion cards, providing another 20 channels, Figure 26.b).

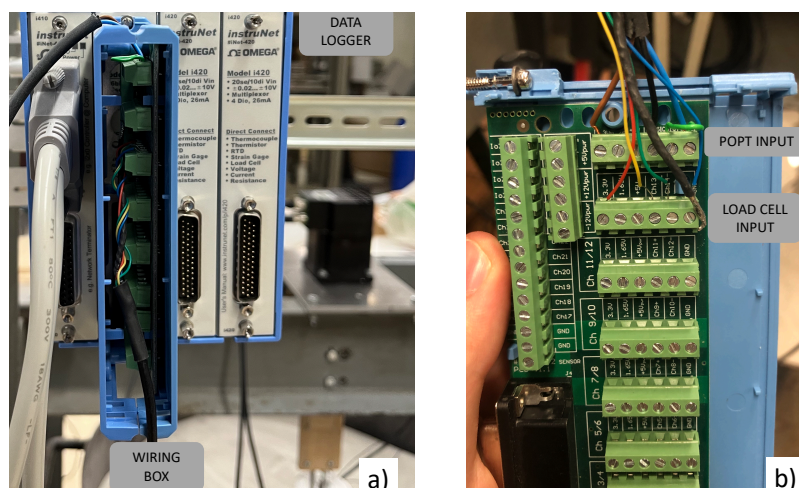


Figure 26 - (a) View of Data Logger and (b) Internal view of iNet-412 wiring box

The data logger is connected to a computer running the *InstruNet-W+* control software where the signals from the attached sensors are captured and presented as parameter vs time plots in real-time, e.g, as shown in Figure 27.

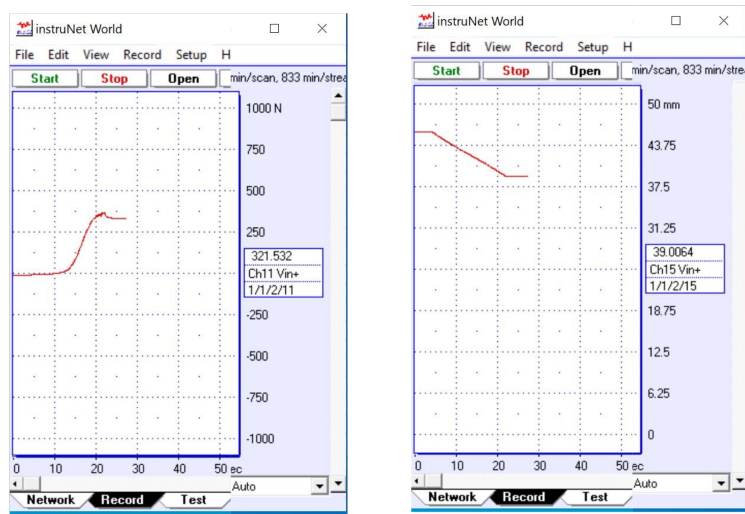


Figure 27 - *InstruNet-W+* control software interface capturing (a) load and (b) displacement vs time plots in real-time

In addition, the software allows the record of displacement and load readings to be exported in various file formats, including .xls (Excel). This enables the plotting of several types of graphs i.e., load-time, displacement-time and load-displacement (see examples shown in Figure 28), which are essential to handling data and interpreting the results of the tests.

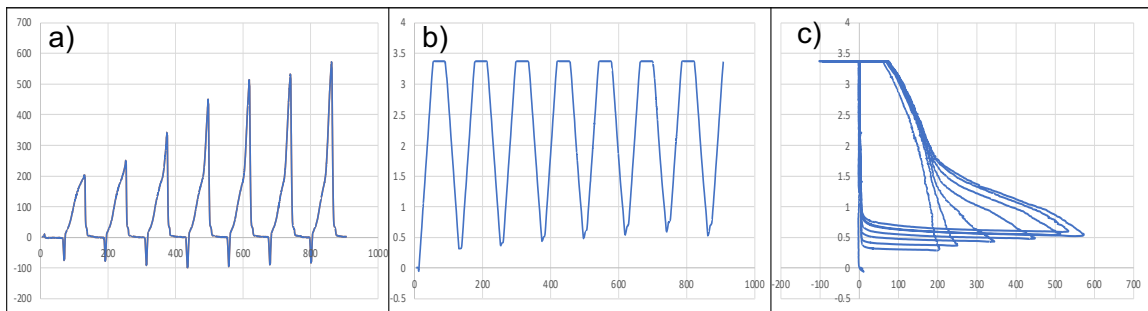


Figure 28 - Initial tests graphs: a) load-time, b) displacement-time and c) load-displacement (units in N, s and mm)

4.1.6 Tank

The tested pile and sand were setup inside the steel tank shown in Figure 29. The tank is a Chapter of used pile casing with a nominal diameter of 750 mm and was donated by a local piling company. Averaging several measurements along its length, the cylindrical tank, that has a diameter of 765 mm and is 905 mm long.

The width of the tank ensures a tank radius to pile radius ratio of 19.1, which is sufficient to minimise the potential for interference between the pile and the tank walls. The height of the tank ensures that after allowing up to 100 mm freeboard between the sand filling and the top of the tank, and with 600 mm pile embedment, the minimum distance between the pile base and the tank base is at least 200 mm, or 5 times the pile diameter which should ensure that there is minimal interference between the tank base and the pile base failure mechanism.

Each set of tests would involve the filling of the tank with, approximately, 450 to 500 kilograms of dry sand, depending on the soil preparation method. In order to help in some soil preparation methods, layers of 50 mm each were marked inside the tank. Also, to facilitate the emptying, a small trap door was created in the wall of the tank.

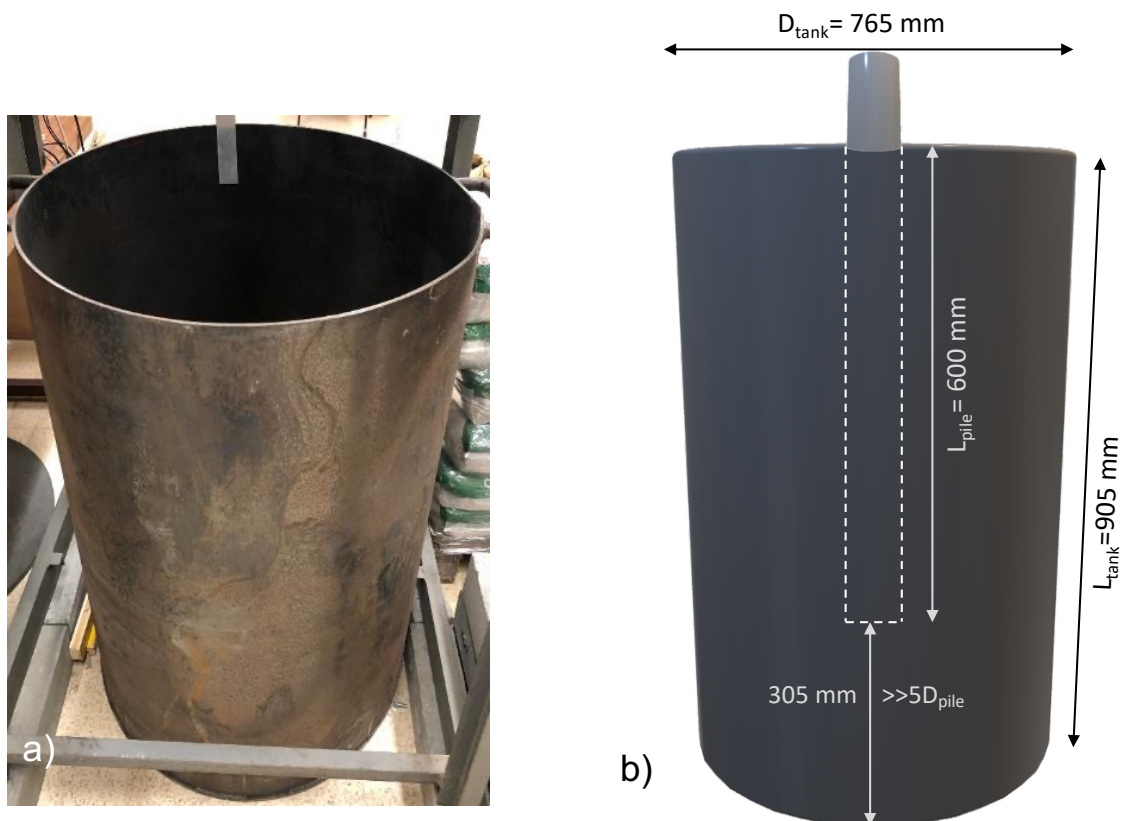


Figure 29 - (a) Tank used for the experimental campaign; (b) Tank dimensions

4.2 MATERIALS: SOIL

The goal of this dissertation was to study the pile response to cyclic axial loading in a dry granular soil, Figure 30. This was chosen largely for convenience and to avoid working within with a wet environment. The soil used is identified as *APAS 30* by the supplier *Areipor - Areias Portuguesas S.A*, which has been used regularly within the laboratory in the past. According to their technical sheet (Appendix C), the material consists of a “sand with presence of

quartzite, quartz, and feldspar. Particles with a sub-prismatic, sub-angular shape and with a slightly rough surface". To guarantee controlled conditions, a series of classification tests were undertaken and Table 7 summarises the soil parameters obtained. Details of the tests undertaken are provided in the following Chapters.

Once this is a small-scale model testing, to limit the effect of grain size on the peak shaft resistance, Garnier et al., (2007) recommends that the ratio of the model pile diameter to the d_{50} , D/d_{50} , for the soil should be between 50 and 100. In this study, the ratio is $D/d_{50} = 69$, which is considered satisfactory. At the time this work was undertaken, it was envisaged that soil element testing might be undertaken to define e.g. the shear strength characteristics of the soil and soil-pile interface, and advanced parameters for numerical modelling. However, this was not done due to the unavailability of equipment at the time and is planned for a later date.

Table 7 - APAS 30 soil parameters

Soil Parameters	Unit	Value	Test Standard
Particle size 10%-passing, d_{10}	mm	0.425	E 239-1970
Particle size 60%-passing, d_{60}	mm	0.6	
Coefficient of uniformity, $C_U = d_{60}/d_{10}$	-	1.41	
Particle size 50%-passing, d_{50}	mm	0.575	
Particle density, ρ_s	Mg/m ³	2.66	NP-83 (1965)
Specific Gravity, G_s	-	2.66	
Maximum dry unit weight, γ_d^{\max}	kN/m ³	14.3	Non-Standard
Minimum dry unit weight, γ_d^{\min}	kN/m ³	13.7	ASTM D4254-16
Minimum void ratio, e_{\min}	-	0.89	
Maximum void ratio, e_{\max}	-	0.825	Non-Standard



Figure 30 - APAS 30 Sand

4.2.1 Particle size distribution

The particle size analysis is a measurement of the distribution of average particle sizes in a soil sample. The Portuguese Standard E 239-1970 for determining the particle size distribution using the wet sieving technique. This specification details the procedure to be followed, in which the soil is forced to pass through a series of standardised ASTM (American Society for Testing and Materials) sieves with, successively, finer mesh sizes. The retained material is weighed to find out what percentage it represents of the total weight, which then allows the percentage of material passing each sieve to be determined. The results of this analysis can be found on Appendix D and Figure 31 presents the resulting particle size distribution curve.

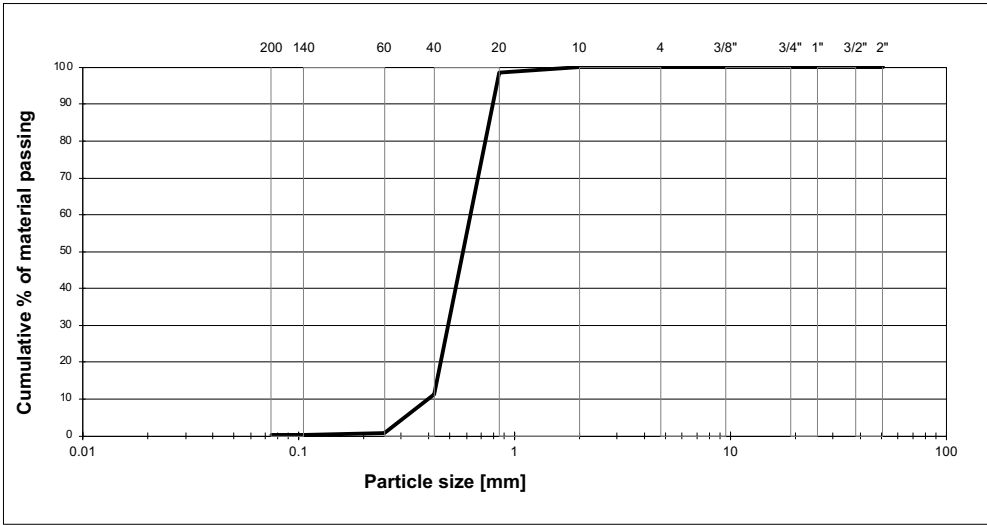


Figure 31 - Particle size distribution curve for APAS 30

The particle size distribution curve exhibits a narrow range of particle size distribution, corresponding to a uniform granulometry ($C_U = 1.41$). Namely: 99% of the APAS 30 has size between the no. 60 (0.25 mm) and no. 20 (0.85 mm) ASTM sieves. Out of which, 90% of the particles stay in the range between the ASTM no. 40 (0.425 mm) and no. 20 sieves. According to the ASTM D2487-17, APAS 30 is categorized as a Medium Sand, which means the majority of the material passes a 2.00-mm sieve (No. 10) and is retained on a 0.475-mm (No. 40) sieve.

4.2.2 Particle density, ρ_s

The particle density of a certain soil, ρ_s , expresses the ratio between the weight of a soil sample and the volume occupied by this solid fraction, without considering porosity. This parameter, whether the soil is dry or wet, remains always the same, as long as the weight of the water contained is subtracted from the mass of the sample.

The Portuguese Standard NP-83 (1965) establishes the procedure to be followed, which involves a small pycnometer, a scale reading to 0.01 g, a recipient, distilled water and a thermometer, as shown in Figure 32, and takes about 13 hours, as the soil has to sit in an oven. The procedure was repeated three times, to confirm whether the values are similar and ensure the test was done consistently. A mean of the 3 obtained values was made and the results can be found on Appendix E. Finally, the value for ρ_s obtained for the APAS 30 is **2.66** (Mg/m^3), which is a consistent value for a non-organic soil and is numerically equivalent to the Specific Gravity of the soil particles, G_s .

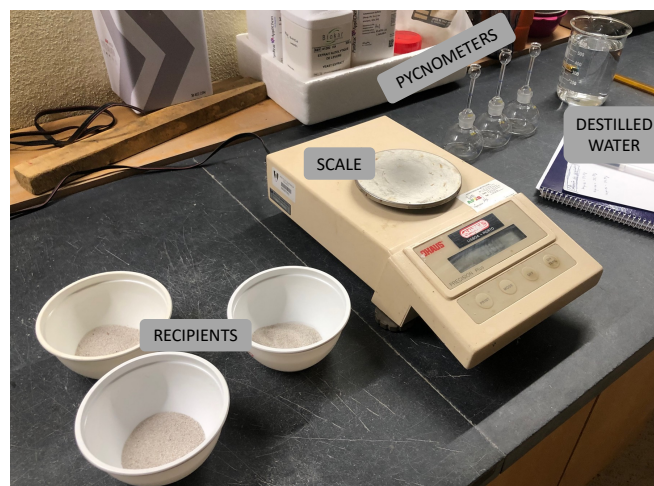


Figure 32 - Particle density test materials and equipment

4.2.3 Minimum dry density / unit weight

To estimate the minimum dry unit weight for the APAS 30 sand, ASTM D4254-16 and BS 1377-4:1990 were used to obtain complementary values.

The minimum dry unit weight, γ_d^{min} represents the loosest condition of a cohesionless soil that can be attained by a standard laboratory procedure that minimizes compaction of the soil. The method A of ASTM D4254 was used in which the sand is poured carefully into a standard cylindrical vessel to minimise the fall height. The procedure was repeated three times, and the mean of the 3 values made. The value for γ_d^{min} of 13.7 kN/m^3 was obtained.

BS 1377-4:1990 defines another way of obtaining the γ_d^{min} of a granular soil, which was also performed, to compare with what had been obtained with the ASTM D4254 method. This approach is similar to Method C of ASTM D4254 and involves turning upside down a sand sample inside a glass measuring cylinder, to produce the loosest possible sample. The value of γ_d^{min} of 13.5 kN/m^3 was obtained for the APAS 30, which is consistent with the value obtained by the ASTM method.

The void ratio, e , defines the ratio between the void volume of a soil sample and the volume occupied by it. Based on a value of γ_d^{\min} of 13.7 kN/m^3 , for $\gamma_s = 26.1 \text{ kN/m}^3$, the minimum void ratio, e_{\min} is obtained as follows:

$$e_{\min} = \gamma_s / \gamma_d^{\min} - 1 = 0.905$$

4.2.4 Maximum dry density / unit weight

The maximum dry unit weight, γ_d^{\max} , represents the densest condition of a cohesionless soil that can be attained by a standard laboratory procedure. To estimate the maximum dry unit weight for the APAS 30 sand, no standard was used, an approach suggested by the laboratory technician was used instead.

In this non-standard approach, the sand is compacted into a standard cylindrical vessel, using a tamping rod. The procedure involved filling up the vessel by 3 layers and compacting each layer 25 times with the tamping rod. After doing so, the top layer is smoothed with a spatula and the set vessel + compacted sand is weighed with a scale, obtaining γ_d^{\max} .

The procedure was repeated 3 times and, once the values were persistent, a final value for γ_d^{\max} is obtained. The test values were obtained for $\gamma_d^{\max} = 14.3 \text{ kN/m}^3$ and e_{\max} as follows:

$$e_{\max} = G_s \gamma_w / \gamma_d^{\max} - 1 = 0.825$$

4.3 SOIL SAMPLE PREPARATION METHODOLOGY

Based on the soil classification testing detailed in the previous Chapter, a target soil unit density of 14 kN/m^3 , representing a relative density, D_r , of 50% was chosen. To ensure that this could be achieved and to confirm that the soil could be prepared consistently and uniformly within the test tank, a set of trial fillings of the tank were undertaken.

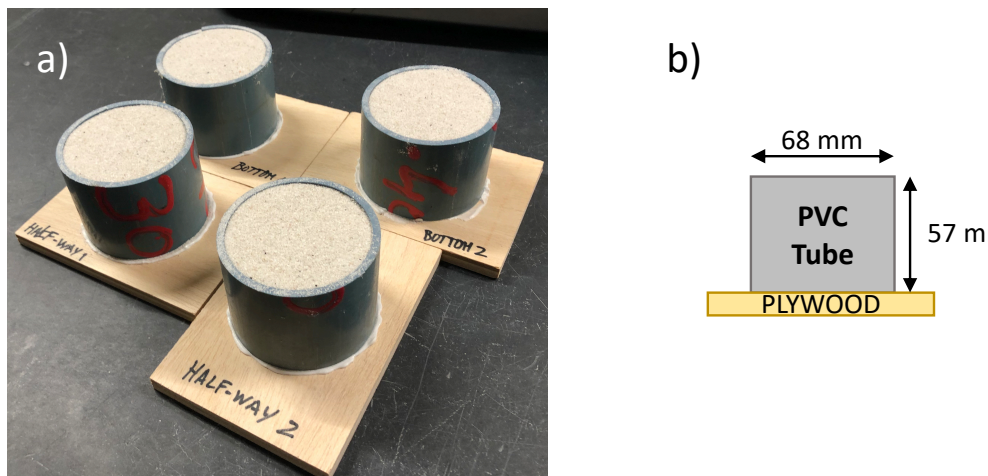


Figure 33 - (a) Sampling cups for sand density control and (b) dimensions

To check the uniformity of the tank filling, a set of four cups (Figure 33) were made by gluing 57 mm-long sections of 68 mm diameter PVC tube to plywood bases. The internal volume of each cup was measured and recorded, along with the total weight of each cup.

During the filling trial, two cups were placed in the bottom of the tank and two about half-way up and were filled as the sand was placed into the tank, Figure 34. After the trial, the cups were carefully exhumed, to minimise further compaction of the sand sample obtained, and weighed. Based on this information, the density of the sand within the test tank was able to be checked.

The results of these filling trials can be found in Table 8, and demonstrate that an initial unit weight, in the range of 13.87 to 14.14 kN/m³ ($D_r = 39$ to 77%) was achieved, which was deemed reasonable.

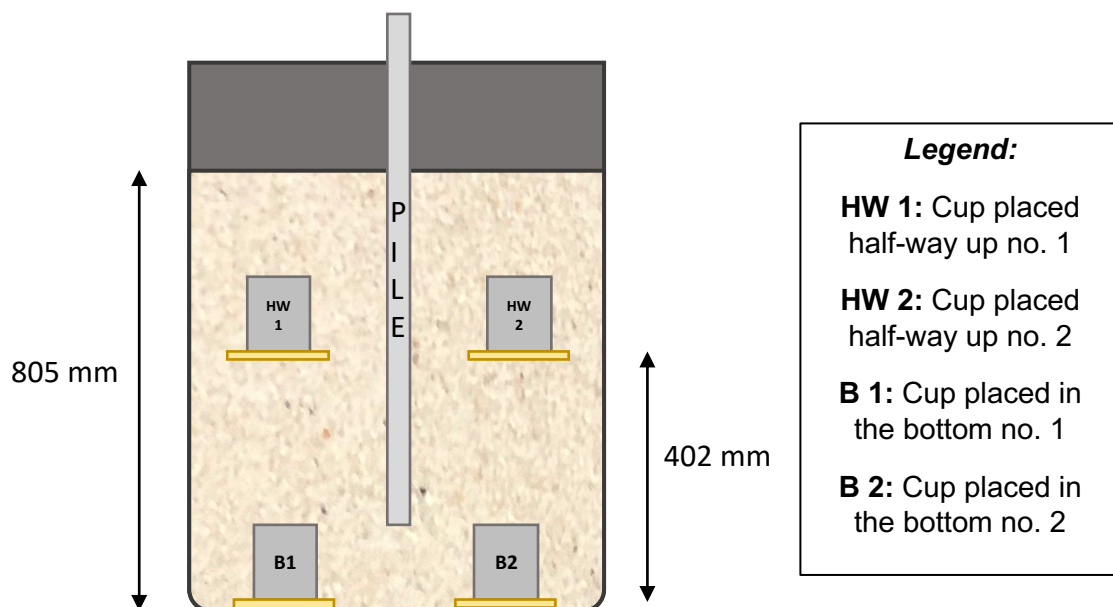


Figure 34 - Sampling cups for sand density control put in place

In some of the preliminary pile tests reported later, two initial states were targeted – dense and loose. The following procedures were used to achieve the target initial states:

1) Compacted sand: the tank is filled with sand in 50 mm thick layers, which were each compacted with a tamper (5.6 kg, 155 mm diameter, 10 blows, fall of 400 mm) to create a dense sample. The tamper used had to be small, since there was little headroom, which was limited by the steel loading frame.

2) Air-pluviated sand: the tank is filled with sand poured through a 35 mm diameter plastic tube and falls into place from a height of about 10 cm. A 10-cm-long guide wire was attached at the end of the tube to ensure the consistent fall height, Figure 35.

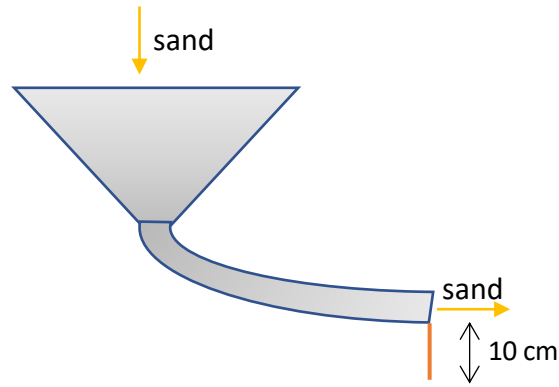


Figure 35 - Funnel and tube used for a loosened sand preparation

The sampling cups were put in position (see Figure 34) to verify the soil density achieved in each trial and Table 8 summarises the density measurements made in the tests. The dense sand had a relative density of 77% which is at the high end of the usual range for dense soil ($D_r = 60$ to 80%) and the loose sand, 39% which is at the high end of the range usually quoted for loose soils ($D_r < 40\%$).

Table 8 - Sand unit weights obtained in sample preparation trial

Position	Units	Dense Sand	Loose Sand
Average unit weight at tank half height	kN/m ³	14.07	13.76
Average unit weight at tank base	kN/m ³	14.21	13.98
Average unit weight	kN/m ³	14.14	13.87
Relative density	%	77	39

It is acknowledged that, even in the loose sand, the material tends to be denser at lower strata, which can be explained by the fact that the overlying sand weight has compacted the particles underneath it, as well as the height at which the sand was poured may end up being higher than intended. It is considered, however, that the effect of the vertical variation of 1-2% in the achieved density will be negligible.

4.4 SENSOR CALIBRATION

In the test setup, a displacement transducer (POPT) and load cell have been utilised in order to measure the model pile response under axial load. While these have been factory calibrated, it is good practice to verify the calibration as part of the testing program.

4.4.1 Displacement transducer

In order to verify the POPT calibration, a known displacement needs to be applied and measured by a micrometre, Figure 36.

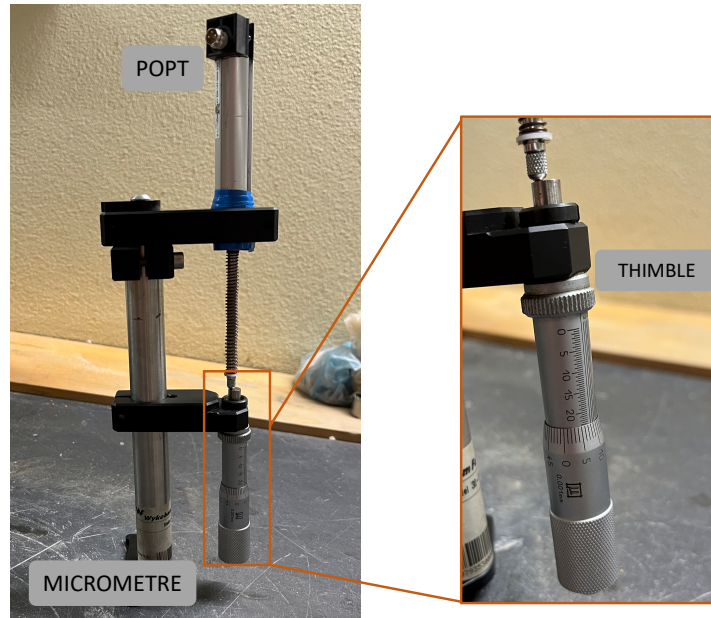


Figure 36 - POPT calibration using a micrometre

The micrometre used for calibration was a *Wykeham Farrance*, model 30-WF0652 (resolution to 0.001 mm) with a range of ± 12.5 mm. The calibration process is simple: after attaching and fixing the POPT to the micrometre, the tip of the displacement transducer sits on the spindle. On micrometre, the exact displacement can be adjusted by turning the thimble, Figure 36. By adjusting the displacement on the micrometre in increments of 5 mm and comparing it with the readings transmitted to the data logger with an error linear trend line, the systematic error found was 6.9%. For example a 1 mm reading is, in fact, about 1.07 mm. It is important to bear in mind that in the laboratory, no measurement is exact, because there are errors that affect the results, and the POPT is no exception.

The error value estimated was considered by applying the correction factor of 1.069 hereinafter to all displacement values recorded.

4.4.2 Load cell

In order to verify the load cell calibration, a known static load needs to be applied in both compression and tension. Due to the length of the model pile, this check was not able to be made at the time the reported testing was undertaken, due to a lack availability of a suitable load frame. However, in the meantime, a static loading system has been fabricated for the existing load frame and the calibration exercise will be implemented in the near future.

4.5 PILE TESTING METHODOLOGY

The philosophy adopted in this study was that, while it is acknowledged that testing under 1g conditions implies that many model scaling effects are not satisfied, the testing is, however, undertaken within a consistent and controlled system, which will allow the stability of a single pile under cyclic mechanical (this study) and thermal loading (not approached in this study) to be appraised.

It was also important to ensure that the tests were undertaken in a consistent manner, to ensure the soil initial state was achieved repeatedly (Chapter 5.3) and to ensure the pile load test was executed in a repeatable manner too. The small-scale model testing of the pile consists of the co-ordinated use of all the equipment and materials described in the preceding Chapters. Although the setup may look complex, it is quite simple. In fact, to run a test, the following steps were followed (Figure 37):

- 1) The tank is filled with sand using the methodology developed in Chapter 5.3, until the level reaches the base level of the pile, then the pile is hung centrally in the tank and the remaining sand deposited while pile verticality is checked at intervals;
- 2) The POPT and load cell sensors are connected to the data logger. The data logger is turned on and the data capture parameters (*Points Per Scan, Number of Scans, Sample Rate, Scan Mode*) are confirmed, in accordance with the created *Running Tests Checklists* on Appendix A;
- 3) The Stepper motor is programmed to load the pile in the planned manner;
- 4) The data logger is started and the motor program is executed: while the POPT measures the pile head displacement, the load cell measures the load generated at the pile head, in response to the imposed displacement;
- 5) The sensor data is captured, at a rate of 20 samples per second, and transferred from the data logger to the computer, where it is visualised as the test proceeds and converted directly to excel format for later analysis;
- 6) The motor program stops automatically as programmed, the data logger is stopped manually, and the next test is readied – returning to either Step 1 or Step 3.

Only after assembling all the hardware as well as mastering the software, were some preliminary tests able to be run and Table 9 summarises the tests, in chronological order, discussed in the next chapter.

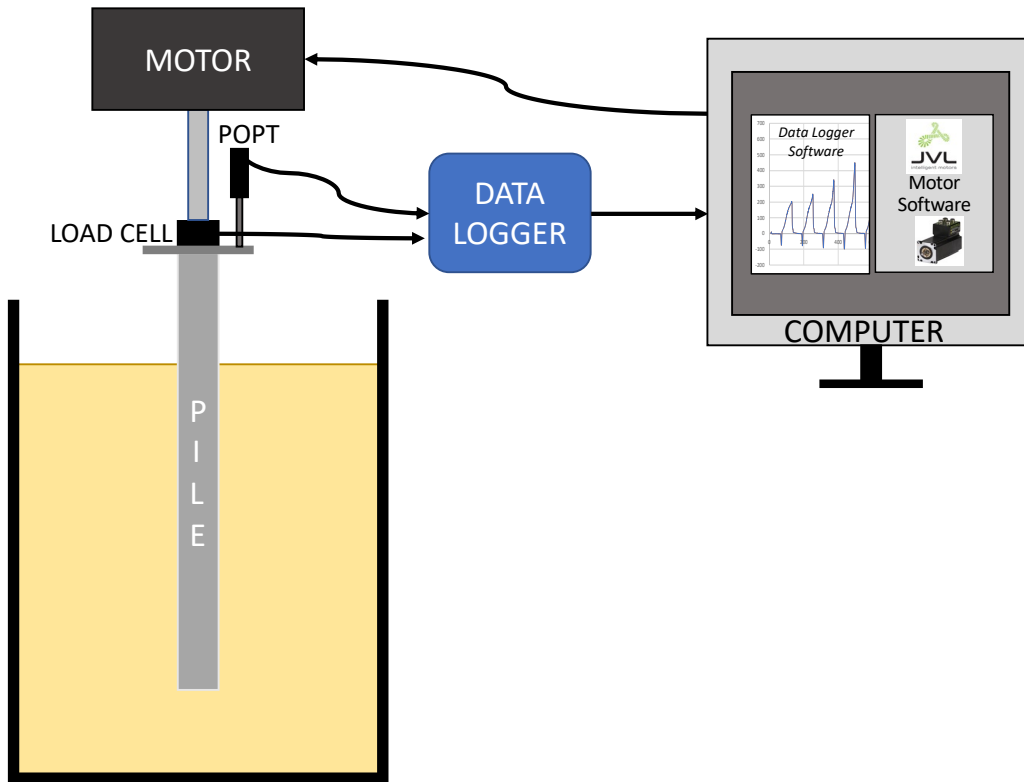
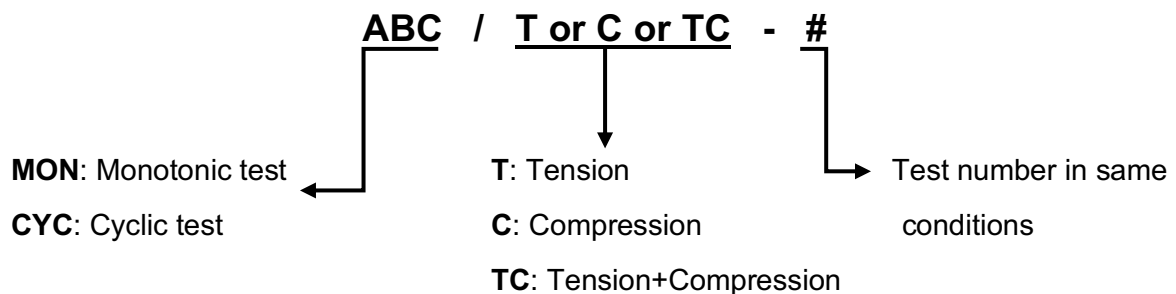


Figure 37 - Schematic of laboratory setup

In order to distinguish the different tests, from this moment forth, the following nomenclature is used:



For example: CYC/TC-3 corresponds to a cyclic test, composed by tension and compression stages (*two-way*), having been the third test to be run in these conditions.

In this experimental campaign, all the cyclic tests that took place were *two-way* tests, therefore, every CYC test will be, inevitably, TC tests as well.

Table 9 - Summary of the model pile tests executed, in chronological order

Test ID							
MON/C-1	MON/T-1	MON/C-2	MON/T-2	MON/C-3	MON/T-3	MON/T-4	MON/C-4
CYC/TC-1	CYC/TC-2	CYC/TC-3	CYC/TC-4	CYC/TC-5	CYC/TC-6	CYC/TC-7	CYC/TC-8

5 TEST RESULTS & DISCUSSION

During an experimental campaign, several unknowns and uncertainties may come up, especially when there are several things one cannot control. Throughout this chapter, initial tests are described, including the necessary preparations for it. These tests are particularly useful to localise what can go wrong, what can go better and how to enhance the quality of the experimental tests. Table 10 summarises the parameters for each of the tests discussed in this Chapter.

Table 10 - Summary details of model pile tests executed

Test ID	D _r	Displ. rate	Max Load	Min Load	Max. Displ.	Min. Displ.	Soil Initial State
	(%)	[mm/sec]	[N]		[mm]		Dense/Loose
MON/C-1	39	0.088	427		13.8		Loose
MON/T-1			-14		15.1		
MON/C-2			801		13.8		
MON/T-2			-388		30		
MON/C-3			800		29.4		
MON/T-3			-399		30.6		
MON/T-4	77		-783		30.2		Dense
MON/C-4			1265		10.7		
CYC/TC-1	77		862	-64	5	3.6	Dense
CYC/TC-2			505	-12	4.8	4.1	
CYC/TC-3			408	-7	4.9	4.2	
CYC/TC-4			405	-2	4.9	4.4	
CYC/TC-5	39		489	-142	4.6	4.1	Loose
CYC/TC-6			561	-2	4.9	4.1	
CYC/TC-7		585	-2	3.3	3		
CYC/TC-8		584	-1	3.3	3		

5.1 MONOTONIC LOAD RESPONSE

Although in Chapter 2 the pile-soil monotonic response is described, it is now the occasion to see this interaction, through the test setup in the laboratory depicted in Chapter 4. Eight monotonic tests were performed, either in tension or compression. While there were still several unknowns about operating the equipment and which results to aim for, the one acknowledged goal was to reach a displacement larger than 20% of the diameter of the pile, i.e. 8 mm, since it is a common criterion for the total mobilisation of the shaft and base resistances leading, ultimately, to failure, as scrutinised earlier in Chapter 2.3.2. One thing to bear in mind is that the stepper motor (or the overall test setup) was found to be malfunctioning, since the commanded displacement does not correspond to the actual displacement, therefore varying randomly, as it is shown in this Chapter.

5.1.1 Estimation of monotonic ultimate load, according to the EN 1997-1

Considering the uncertainties and the unknowns around the pile resistance and, it was considered relevant to estimate the monotonic ultimate load, considering the EN 1997-1 approach described in Chapter 2.3.1.

It may be difficult to assess all the parameters necessary to estimate the ultimate resistance mentioned in Table 1, but since this was only an estimation to guide the experimentally attained loads, the parameters did not need to be extremely precise. In Table 11, these parameters are summarised for dense and loose soil conditions, as well as the estimation of the expected values for the ultimate resistance in compression and tension.

Table 11 - Model parameters and ultimate load estimation according to the EN 1997-1

Parameters	Dense conditions	Loose conditions
$K_{s,i}$	1	0.5
δ_i [°]	35	32
$\bar{\sigma}'_{v,i}$ [kN/m ²]	4.3	4.2
N_q	50	35
$\sigma'_{v,b}$ [kN/m ²]	8.5	8.3
R_s [N]	196	86
R_b [N]	408	280
$R_{c,u}$ [N]	604	366
$R_{t,u}$ [N]	196	86

Therefore, the estimations for the ultimate loads in compression and tension are, respectively, 604 N and 196 N in dense conditions, and 366 N and 86 N in loose conditions.

5.1.2 MON/C-1, T-1 & C-2

For this set of three tests, the sand was prepared in a loose state, with an initial unit weight of 13.9 kN/m^3 ($D_r = 39\%$), as described in Chapter 4.3. The three tests were run one after the other, which means that the final conditions of the first test are the initial conditions of the second test, and so on. The data acquired through the sensors allowed three types of graphs to be plotted, namely: load-time; displacement-time and displacement-load, as shown in Figures 39 a), b) and 40, respectively.

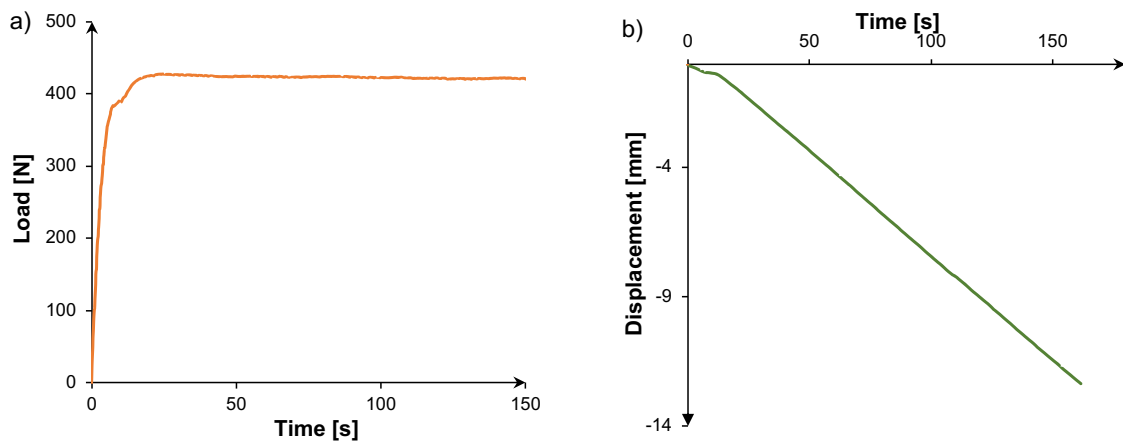


Figure 38 - (a) Load-Time and (b) Displacement-time graphs, MON/C-1

In MON/C-1, the motor was instructed to move 15 mm downwards, to load the pile in compression at a rate of 0.082 mm/s , or 4.9 mm/min . However, failure seems to take place at around 1.3 mm, at a load of approximately to 425 N, Figure 40. Although the shape of the curve appears to be regular, the displacement-pile diameter ratio looks unusual, since it means that full $R_{c,u}$ is fully mobilised at a settlement equivalent to $3.3\%D$, while the expected value would be around $20\%D$, as discussed in Chapter 2. Nonetheless $R_{c,u}$ is equal to 425 N, which is comparable to the estimation of 366 N.

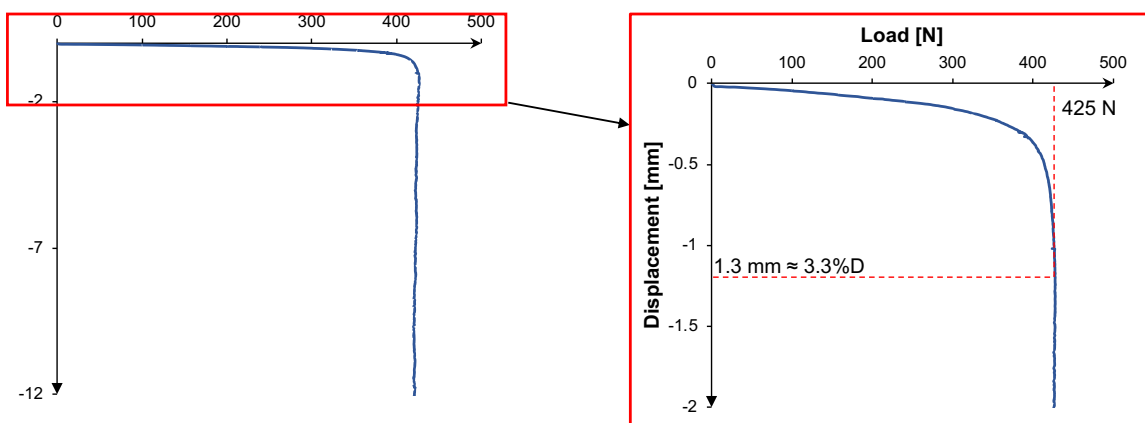


Figure 39 - MON/C-1 Test (a) Displacement-load plot and (b) close-up

Right after running test MON/C-1, the small-scale pile is pulled upwards by 15 mm creating the test MON/T-1, the first monotonic load in tension test. The test did not go as planned and the corresponding displacement-load graphs is very noisy and unstable, Figure 40. It is suspected this instability is related to the lack of torque resistance explained earlier on Chapter 4.1.2.

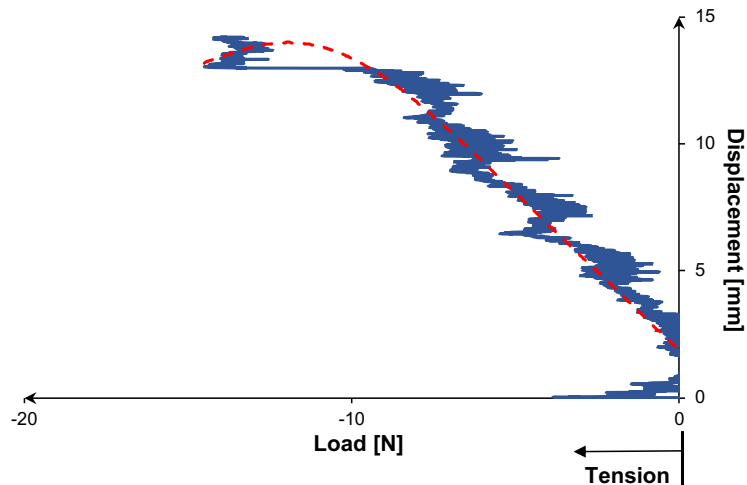


Figure 40 - MON/T-1 Test Displacement-load graph

In Figure 41, an average trend line was plotted in the attempt to try to find a physical explanation for the present test. Since no explanation seemed to be suitable, test MON/T-1 is considered irrelevant and, therefore, shall be ignored.

Right after running test MON/T-1, the pile and soil underwent another compression test about 2 minutes later, MON/C-2. By not altering the soil between tests, this means that the soil final conditions of MON/T-1 are the initial conditions of MON/C-2, which is crucial to understand the load-displacement graph shown in Figure 42.

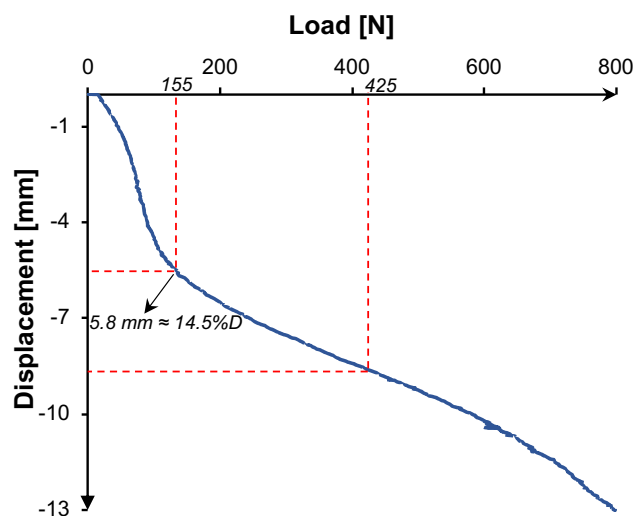


Figure 41 - MON/C-2 Test Displacement-load graph

At first, the curve shape was found to be peculiar, because being this another monotonic compression test, it would be expected the curve to be similar to the first compression monotonic test, MON/C-1. However, when comparing these two tests, MON/C-2 displays a stiffer behaviour by attaining higher loads for equivalent displacements. Even though failure is never attained, it seems to start taking place around 700 N because beyond it, the response appears to be softening, which may be an indicator of approaching failure.

In Figure 42, the load and displacement corresponding to the failure of MON/C-1 were marked, demonstrating the difference in behaviour between these two monotonic tests. What differs MON/C-1 from MON/C-2 is that the pile has been pulled out before (tension test MON/T-1), altering the soil conditions. It is evident then, the contrast between an “intact” soil and a “flawed” one.

The shape of the displacement-load curves starts assuming a “belly” form, reaching the maximum compression load at 800 N. It was perceived that the “belly” shape start is evident at 155 N, or 5.8 mm. A possible assumption for the shape of the curve can be that the soil below the pile is compacted and, as the pile goes upwards and downwards, a blank space is left, so there is “new” soil falling to the pile position as it is being pulled, as simply demonstrated in Figure 43. So, when a compression test is performed after pulling out the pile, the “new” soil is brutally pushed out of the way, to make room for the pile. The “new” soil right after falling to the pile position is loose, so, when compressing it, there will be a first stage (0 to 155 N) of penetrating through the “new soil”, which will eventually compact. Once it is compacted, there is the stiffening of the curve (155 to 800 N), that corresponds to the compaction of the soil that is being compressed.

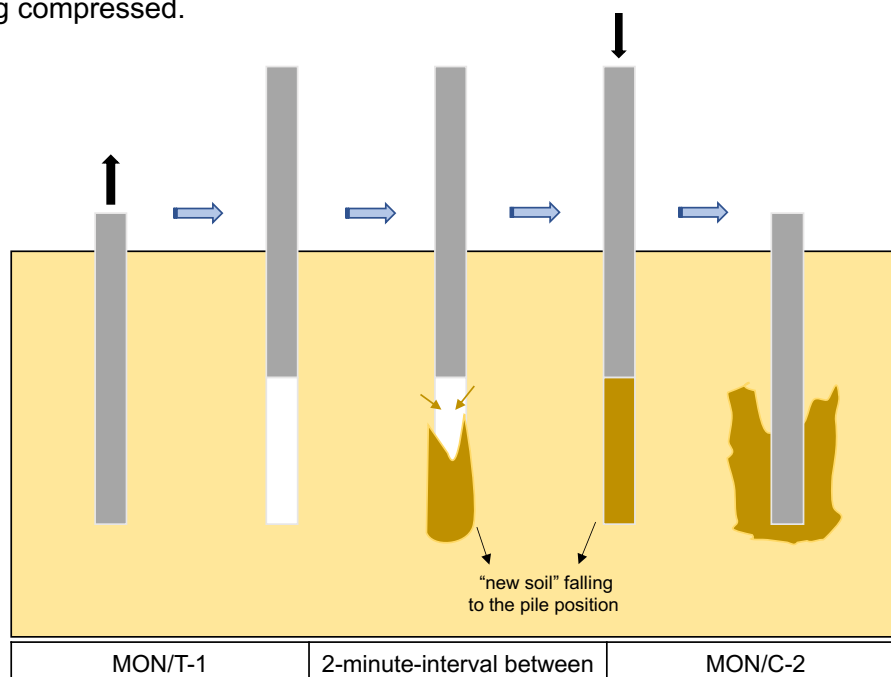


Figure 42 - Conjecture of soil behaviour between MON/T-1 and MON/C-2

5.1.3 MON/T-2, C-3 & T-3

Before this set of three tests, the tank was emptied out and refilled back in, so that the sand was prepared in a loose state. Similarly to Chapter 5.1.1, the three tests were run one after the other, which means that the final conditions of the first test are the initial conditions of the second test, and so forth.

Since MON/T-1 was disregarded because of its irregularity, a MON/T-2 was run, Figure 44.a). In this test, a failure load of 388 N was recorded at about 4%D. Being a tension test, which means only the shaft resistance is mobilised, and considering the soil state (with low confining stress and stiffness of the soil adjacent to the pile), this recorded load was not expected, being almost identical to that obtained in the MON/C-1 (which should include base and shaft components of resistance). Therefore, out of the two scenarios, only one is possible in MON/T-2: either a large portion of the resistance is being mobilised at the base (not only because of the soil preparation, but also because APAS 30 is a very cohesionless sand), or there is none/very little base resistance in compression (which may be due to the test preparation). Also, the estimation for $R_{t;u}$ was about 86 N, which corroborates the fact that the attained resistance of 388 N is partially also being mobilised at the base. MON/T-3, in its turn, provides practically the same values for ultimate load and displacement, as shown in Figure 44.b), even though a compression test, MON/C-3, has occurred between these tests. Therefore, it is unlikely the sand conditions are not equivalent.

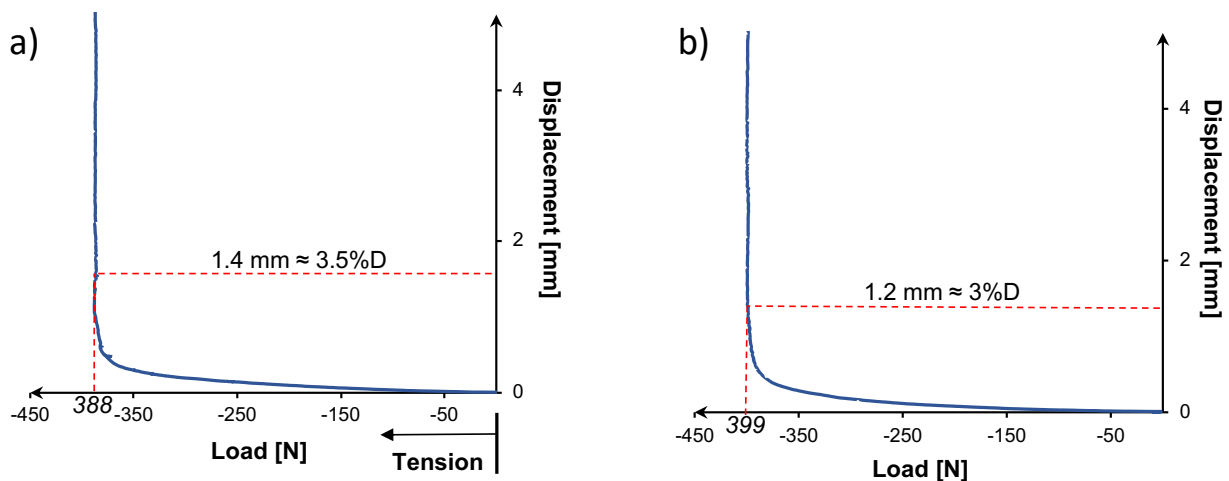


Figure 43 – (a) MON/T-2 and (b) MON/T-3 Test Displacement-load graphs

Test MON/C-3 (Figure 45) took place a couple of minutes after MON/T-2, and the displacement-load curve exhibited a similar response to that previously discussed in relation to MON/C-2. The initial conditions are similar since the soil is altered by having pulled the pile out before compressing it again. The results in Figure 45 are consistent with the ones obtained

in MON/C-2 since the change in behaviour curve occur at around the same load (149 N) and displacement (5.8 mm). The one thing that alters though, is the clearer tendency of curve to plunge, indicating failure at around 800 N, which had not been observed well before. The noise around 700 N is related this instability is related to the lack of torque resistance explained earlier on Chapter 4.1.2.

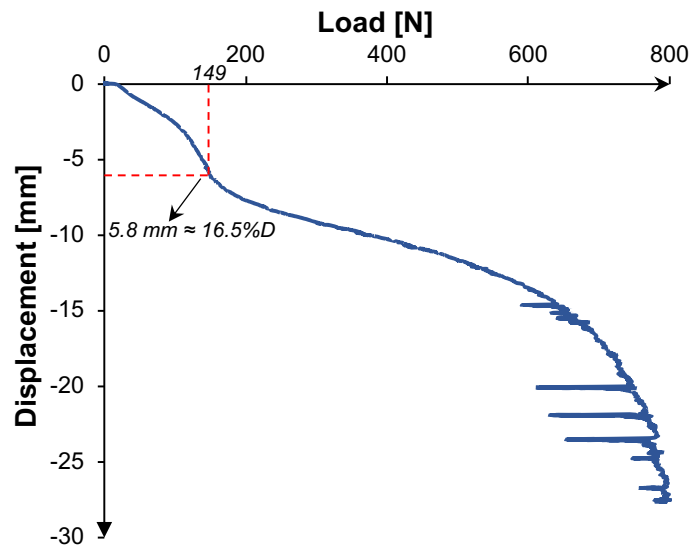


Figure 44 - MON/C-3 Test Displacement-load graph

5.1.4 MON/T-4 & C-4

In contrast to the previous tests, for this set the sand was prepared in a dense state, with an initial unit weight of 14.14 kN/m^3 ($D_r = 77\%$), as described in Chapter 4.3. Considering the initial soil preparation, the response in tension and compression was expected to be stiffer, since the initial level of confining stresses is higher.

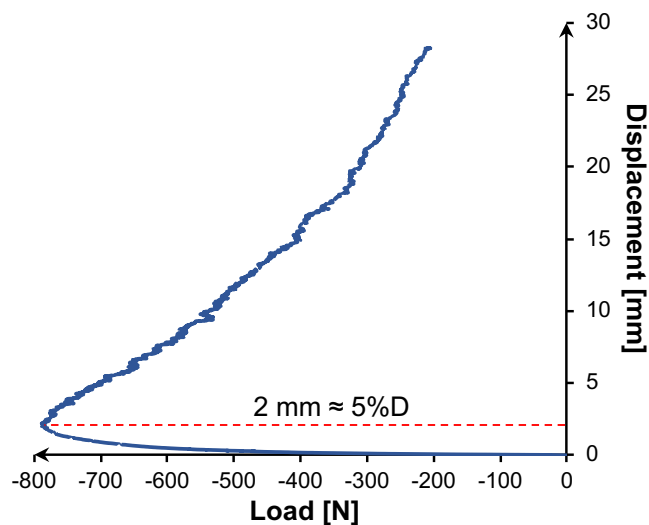


Figure 45 - MON/T-4 Test Displacement-load graph

In MON/T-4 (Figure 46), a load of 800 N is attained at 2 mm displacement, more than twice the recorded ultimate resistance in tension in MON/T-2 and T-3, and therefore not comparable to the estimation of 196 N. However, the response stiffness (load/displacement ratio) is similar to the previous tension tests with an initial loose preparation. The shape of the load-displacement curve is different, exhibiting significant softening after the peak resistance is reached.

By analysing the MON/T-4 curve, it is understood that, due to the method of placement of the sand, the initial confining stresses in the soil adjacent to the pile are higher than in initial tests. So the load necessary to displace it (800 N) will be higher than 390 N obtained previously in the loosen soil. Once the pile moves upwards, the load instantaneously decreases at a rapid rate until the test is finished at 205 N, a reasonable value for failure, considering the estimation of 196 N in Table 11. Further testing would clearly be needed, as to check whether failure would take place around these values.

Afterwards, the test MON/C-4 (Figure 47) was run. Since the response in tension attained already more than twice the monotonic capacity, and, on top of it, the pile has been pulled out the curve behaviour in compression was expected to attain even higher loads and form the “belly” format.

Although the motor was programmed to induce a 15 mm displacement in compression, the test had to be interrupted at 10 mm, shortly after recognising that the load cell maximum capacity of 1000 N had been surpassed.

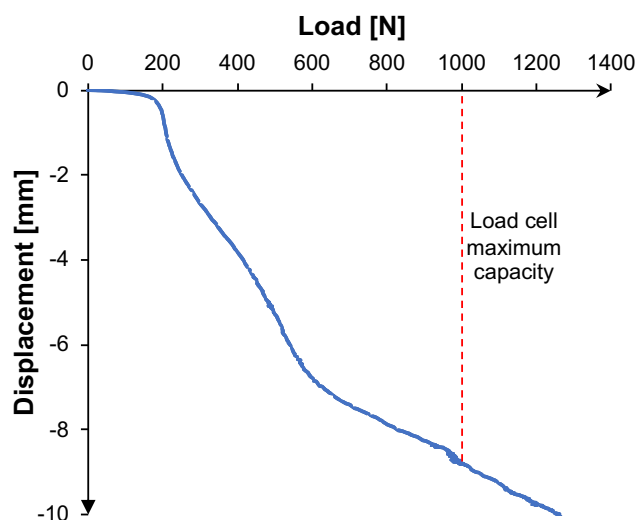


Figure 46 - MON/C-4 Test Displacement-load graph

Even so, there are some/several comments to be written about:

1) between 0 and 200 N, the curve displays an apparent failure, when penetrating the “new” sand that fell to the pile position after being pulled out, this is similar to the earlier tests in loose sand; 2) Between 200 and 600 N the load increases again, but in smaller increments, revealing a less stiff behaviour than between 0 and 200 N; 3) Between 600 and 1200 N the response stiffens, probably because it is penetrating the denser and more compacted lower strata of soil, which had not yet been mobilised.

From these monotonic preliminary tests, one learned about the influence of an “intact” soil and a “flawed” one, since the behaviour of the displacement-load curve changes considerably. Another learning resulting from this Chapter is that the test setup has, indeed, a malfunction, namely the stepper motor. Not only because the induced displacements are not as precise as one would expect, varying in a randomly and with no prediction, but also the lack of torque issue, which could let the pile is slip and create a mismatch between the motor rotations and the pile movement (i.e. the motor keeps turning but the pile does not penetrate the soil).

5.2 CYCLIC LOAD RESPONSE: EFFECT OF SOIL INITIAL STATE

The soil behaviour can be expected to vary significantly depending on its initial state, i.e. as a function of the procedure for placing the sand in the test tank. For these preliminary cyclic tests, two initial states were examined:

5.2.1 Dense sand cyclic tests

In this set of four tests, the sand was prepared in a dense state with an initial unit weight of 14.14 kN/m^3 ($D_r = 77\%$), as described in Chapter 5.3.

As these are preliminary cyclic tests, and there were still a number of uncertainties relating to the equipment and test procedure, as well as how the pile would behave, a limited number of cycles, $N = 3$, were applied.

When running a test, the stepper motor is programmed to follow a set of instructions, such as those shown on Table 12, where the targeted displacement in each stage of the test needs to be expressed as a count number in the motor control software. During these initial tests, it was decided to start with an upwards displacement (tension) with the aim of quantifying the shaft resistance on the pile.

A set of four *two-way* cyclic tests with $N = 3$ were run, which means that each cycle has a tension (pull-out) and then a compression (push-in) stage. Between tests, which were spaced

by 10-minute-intervals, the sand was not taken out of the tank and replaced, which means that the final conditions of the first test are the initial conditions of the second test, and so forth. Similarly to the monotonic tests, the data acquired through the sensors allows 3 types of graphs to be plotted, namely: load-time; displacement-time and displacement-load, as shown in Figures 48, 49 and 50, respectively.

Table 12 - Sequence of motor commands for CYC/TC-1 through 4

Cycle no., N	Target response	Motor command
1	+5 mm	+409 600 counts
	wait 1 sec	wait 1 sec
	-5 mm	-409 600 counts
	wait 1 sec	wait 1 sec
2	+5 mm	+409 600 counts
	wait 1 sec	wait 1 sec
	-5 mm	-409 600 counts
	wait 1 sec	wait 1 sec
3	+5 mm	+409 600 counts
	wait 1 sec	wait 1 sec
	-5 mm	-409 600 counts
	wait 1 sec	wait 1 sec

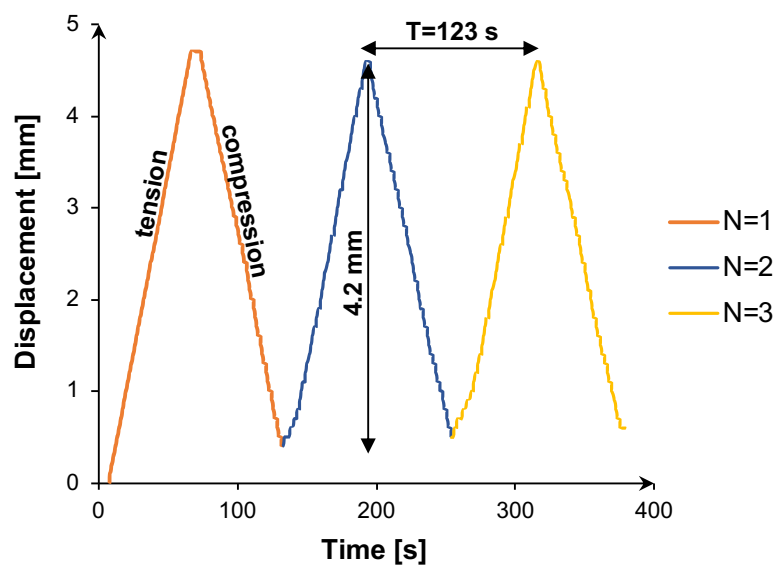


Figure 47 - Displacement-time graph for CYC/TC-1

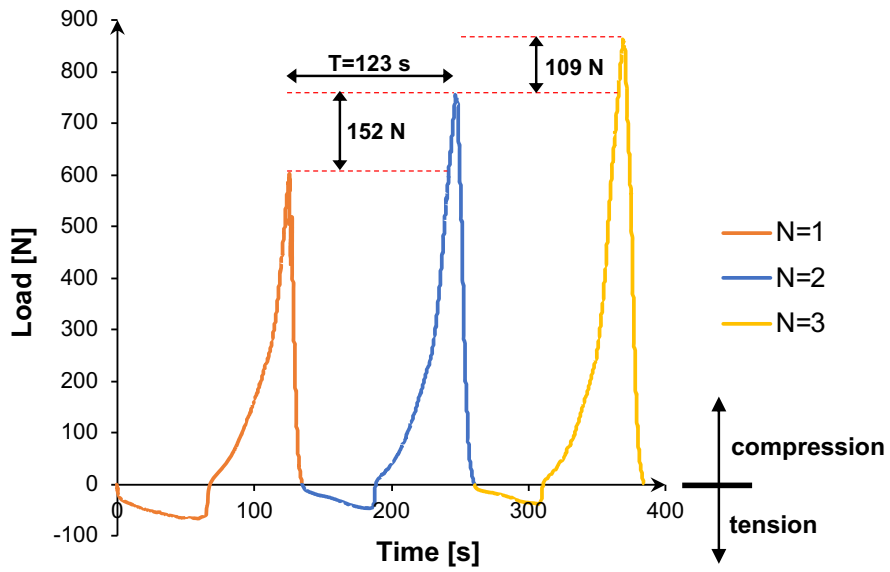


Figure 48 - Load-time graph for CYC/TC-1

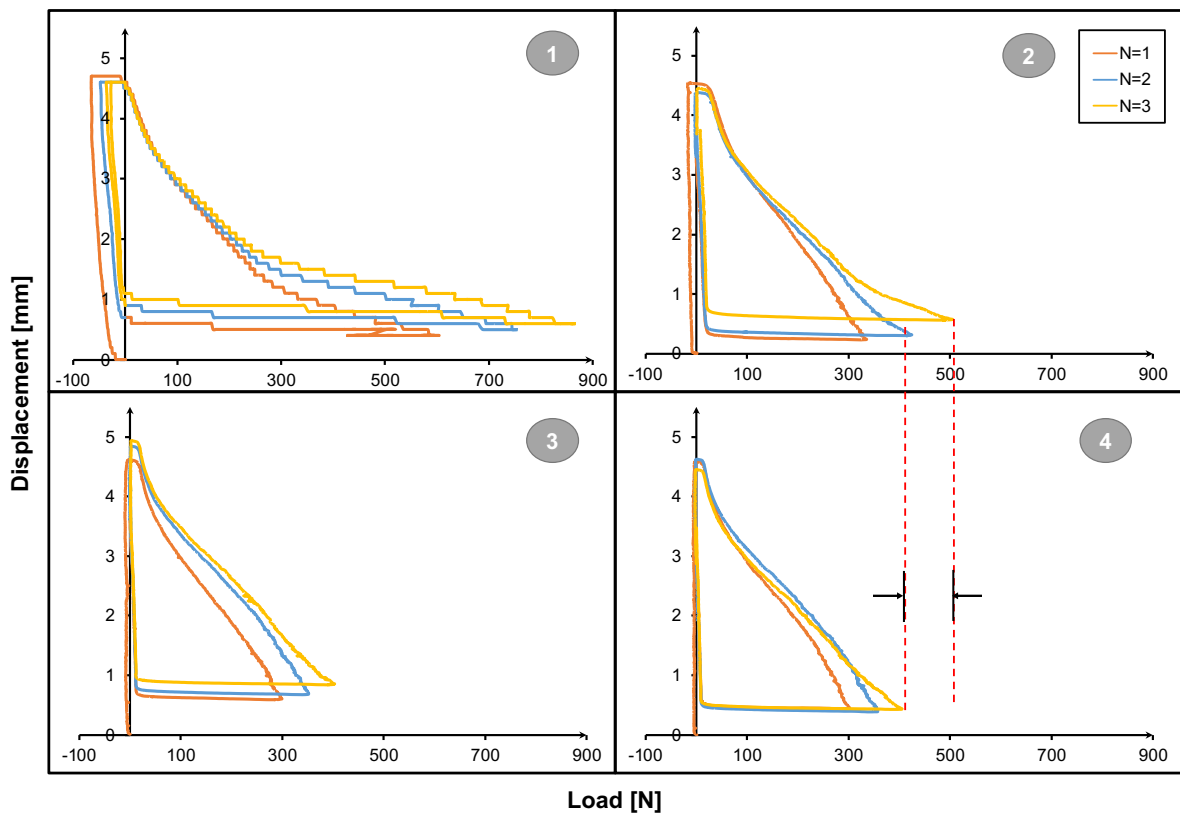


Figure 49 - Load-Displacement graphs for tests CYC/TC-1 through 4 in dense sand

After running the first cyclic tests in dense sand and plotting the corresponding graphs, numerous aspects were noted:

- 1) As shown in the figures, the compression load mobilised is significantly larger than that for tension, because, as discussed previously, the axial compression capacity derives from both the base and shaft resistances, while in tension on the shaft resistance can be mobilised. However, the recorded values for the shaft resistance do not match with those obtained early on the MON test series, and the reason for this remains unknown;
- 2) The period of the cyclic load is 123 s and is kept constant in all 3 cycles of the 4 tests. Since the existing experimental data does not go further than 10 s, this is considered to be a large period;
- 3) Considering this is a displacement-controlled investigation, it is seen the measured displacement, although a somewhat irregular, is consistent. On the other hand, the maximum measured load, within the same test, increases from cycle to cycle;
- 4) Therefore, with the increasing number of cycles, there is a rearrangement of particles, which results in an increase in resistance;
- 5) On tests CYC/TC-2, 3, and 4, the maximum load attained in each test is significantly lower than that of CYC/TC-1. This fact is certainly related to the initial soil conditions, since the first test was the only one to take place right after compaction, hence attaining a higher load;
- 6) Knowing that the period is constant and that a larger displacement takes place in CYC/TC-1, there will be less coordinates to be recorded in between, hence explaining why there is some turbulence when compared to the others;
- 7) There is a permanent increase in stiffness, from test to test, meaning that the load/stiffness ratio increases. As it is noticeable, for a fixed displacement, the corresponding load is higher from test to test, in other words, the behaviour is stiffer;
- 8) From the test CYC/TC-1 to 2, a large fall is seen in maximum load attained, meaning the initial conditions are rapidly degraded. Therefore, this indicates that the graphs will shrink, which they do;
- 7) While within a test, the maximum load attained increases from cycle to cycle, in Figure 51 it is clear that the maximum load attained decreases from test to test. The large drop in resistance from CYC/TC-1 to 2 may reveal that, at least in dense initial conditions, the major loss in resistance takes place in the very first cycle. However, as the number of cycles N and number of tests increase, the maximum load tends to stabilise, especially on the last 2 tests. Further cycles would need to be run, to understand whether this stabilisation is merely apparent or not;

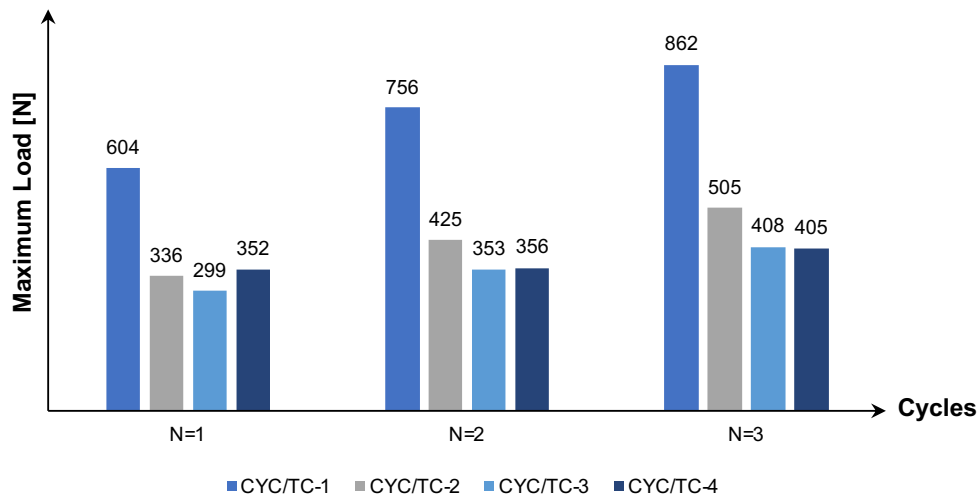


Figure 50 - Variations in maximum attained loads on dense sand test

8) Even though the motor is instructed to move 5 mm, the recorded displacement is different, varying in all cycles and tests. The load cell, in its turn, can present somewhat varying values. The reason for this is not clear, nonetheless it is suspected this is related to the approach used for zeroing the load cell and POPT. In the approach used, the initial recording values are just set to 0, not considering or interpreting which values were being recorded by any sensor, especially the load cell.

For example, if the load cell sensor is recording 7.982 N and, applying the approach of setting all recording values to zero, a -7.982 N is added to all recording values, becoming 0 N the first load recorded by the load cell. However, this 7.982 N initial recorded value (or any other, since it was not constant throughout the experimental campaign) can be related to several factors, such as the own weight of the pile, or the fact that the pile is sitting initially on sand, or both;

9) The initial goal of attempting to identify the mobilised shaft resistance is accomplished, being, approximately, 61 N in the first cycle of the first test. Although the shaft resistance obtained in MON/T-2 was about 390 N, the 61 N appears to be a more realistic estimation, since this is a cohesionless soil, with low capacity of mobilising great resistances along the shaft (and considering the estimation of 196 N obtained earlier). Nevertheless, this mobilised resistance quickly tends to zero, as further cycles and tests are run, proving the phenomenon the shaft resistance of degradation, even though this requires further investigation, Table 13.

Table 13 - Variations in attained loads and displacement on dense sand preliminary tests

Cycles	$\Delta\text{Load_compression [N]}$		$\Delta\text{Load_tension [N]}$		$\Delta\text{displacement [mm]}$	
	1 \rightarrow 2	2 \rightarrow 3	1 \rightarrow 2	2 \rightarrow 3	1 \rightarrow 2	2 \rightarrow 3
Test #1	152	111	19	14	0.1	0.1
Test #2	90	80	7	0	0.1	-0.1
Test #3	52	50	3	0	0	-0.1
Test #4	54	51	2	0	0	0.1

10) Another important aspect is the shape of the curves on Figure 50. The *unexpected* curve behaviour is the “belly” developed around the maximum compression load for each cycle, when the load is relatively high. A possible explanation has been thoroughly discussed in Chapter 5.1.1. However, as more cycles are applied, the curve stiffens, adopting a shape more similar to the monotonic ones plotted previously, as shown in Figure 52.

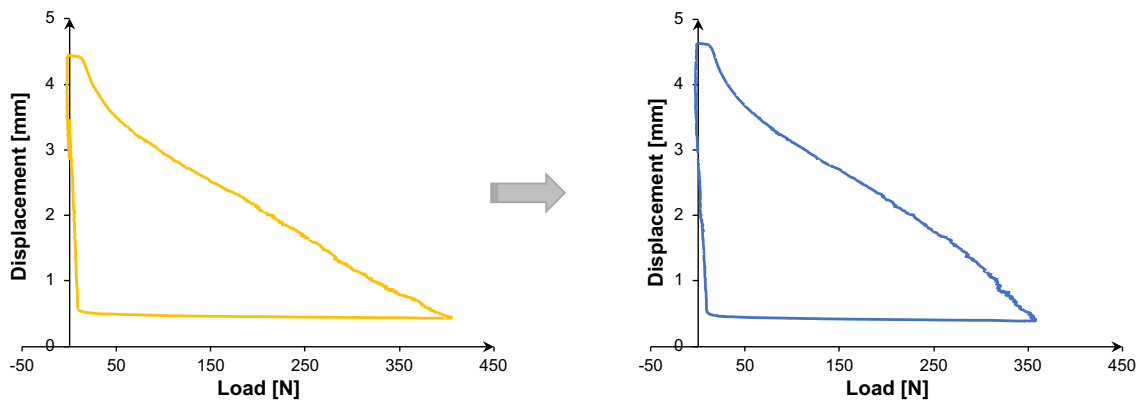


Figure 51 - Load-displacement curves for CYC/TC: 2 & N=3 (left) and 4 & N=2 (right)

In conclusion, these tests on a dense APAS 30 are beneficial for further testing, conveying the impression that increasing the number of cycles, N , can be favourable in the sense that the response is stiffer, although there is a clear loss of resistance from cycle to cycle in test to test.

Therefore, and at least for low values of N , pre-cycling the sand does seem to stiffen the pile-soil response and it increases the level of stabilisation of the maximum load until 400 N is achieved, which is remarkably similar to the ultimate resistance in loose soil. In other words, after cycling the soil with initial dense conditions, the ultimate resistance was similar to the monotonic response with initial loose conditions.

The sand preparation method played a major role in this test, since it allowed the observation of how quick the resistance falls, only after the first 3 cycles being applied. The fact that, within

the same test, the load increases must not be confused with the fact that the load decreases from test to test, for the same cycle, Figure 51.

Although an evident 50% loss in resistance is observed, the tendency of stabilisation around the ultimate static capacity implicates that the cyclic effects were not harmful in the sense that the ultimate barrier was not surpassed. In other words, thinking of a real-world scenario, a pile designed only based on the ultimate static capacity, its failure would likely not happen. Clearly, the loss in capacity shall not be ignored either. Evidently, further investigation is required.

5.2.2 Loose sand cyclic tests

In this set of four tests, the APAS 30 sand was prepared in a loose state with an initial unit weight of 13.87 kN/m^3 ($D_r = 39\%$), as described in Chapter 4.3.

This second set of cyclic tests was slightly modified to build on the experiences from the dense sand tests. Firstly, since the behaviour beyond $N = 3$ cycles remained unknown, a higher number of cycles, $N = 10$ was considered. The main objective being to understand if the pile-soil behaviour stabilises, as it has been reported in the literature. Nevertheless, similarly to the dense sand tests, two-way tests are performed, starting with pile pull-out to quantify the ultimate shaft resistance. The period remained unchanged at $T=123 \text{ s}$, as did the displacement imposed in each cycle, i.e. $\pm 5 \text{ mm}$. As before, after preparing the model in the tank, the four sets of tests were run one after the other without replacing the sand, meaning that the final conditions of test CYC/TC-5 are the initial conditions of test CYC/TC-6, and so forth.

After running the tests on the loose sand, the resulting load-displacement graphs are presented in Figure 53 and various aspects were noted:

- 1) The shape of the load-displacement curves assumes the same “belly” form, when reaching the maximum compression load. Though this time, it is evident that the shape of the curve changes around the 200 N threshold, as marked in Figure 52;

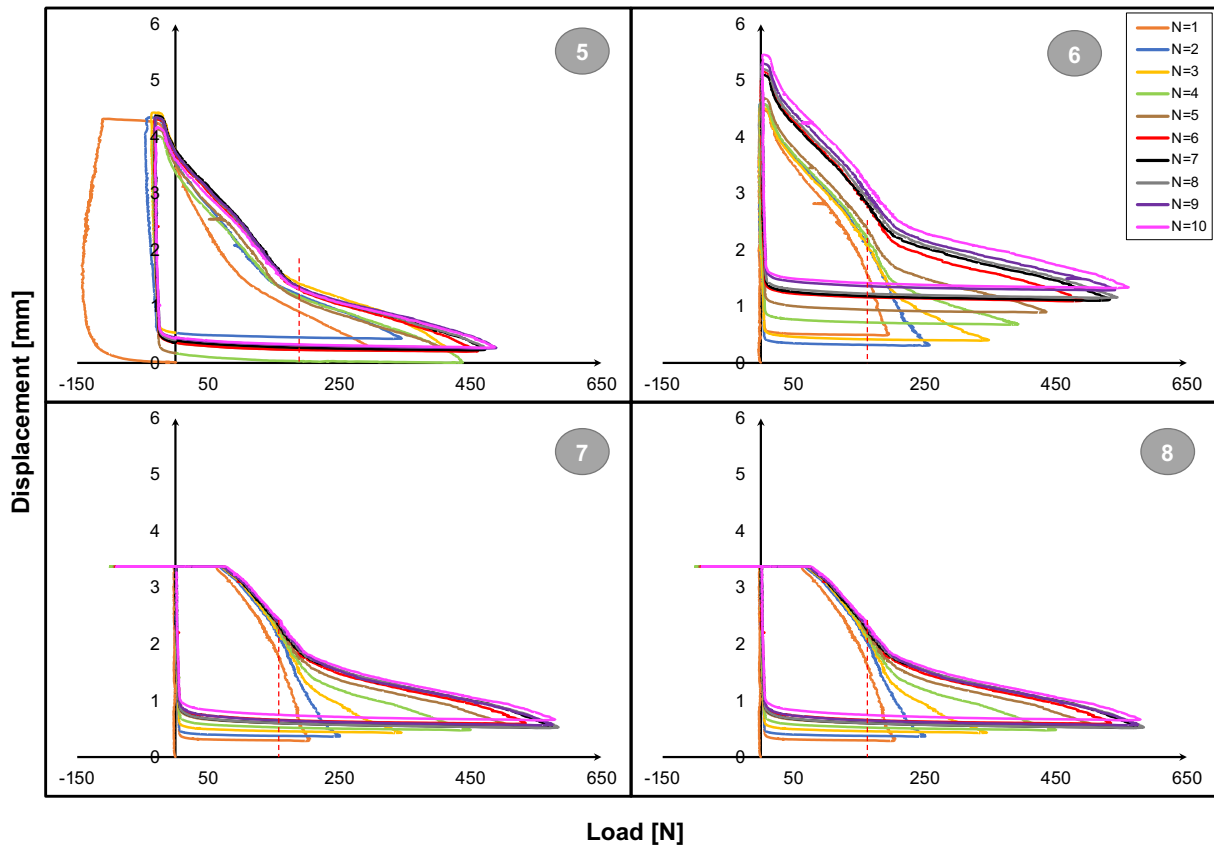


Figure 52 - Load-Displacement graphs for tests CYC/TC-5 through 8 in loose sand

2) Unlike the previous tests, the maximum attained load in the last cycle increases from test to test, as shown in Figure 53. This means that the graphs will successively stretch, as opposed the dense ones, where the graphs would successively shrink, as shown in Figure 53. So, the maximum attained load is greater than the monotonic tests' values as well as the cyclic tests with initial dense soil conditions;

3) Surprisingly, the mobilised shaft resistance on $N = 1$ of CYC/TC-5 is higher in loose conditions than in dense conditions, being around 150 N. Nonetheless, it degrades faster, being almost totally lost by $N = 3$ of the first test;

4) Throughout these tests, the stepper motor is commanded to displace 5 mm, either in tension or compression. Even though in tests CYC/TC-5 and 6 the measured displacement is around 4.2 mm, it is not constant. In fact, in tests CYC/TC-7 and 8, the measured displacement does not even surpass the 3.4 mm. For now, it remains unknown the reason why the motor would stop moving, since its thrust is approximately 2000 N. In later tests, this is an important aspect to be addressed since it might need to be fixed;

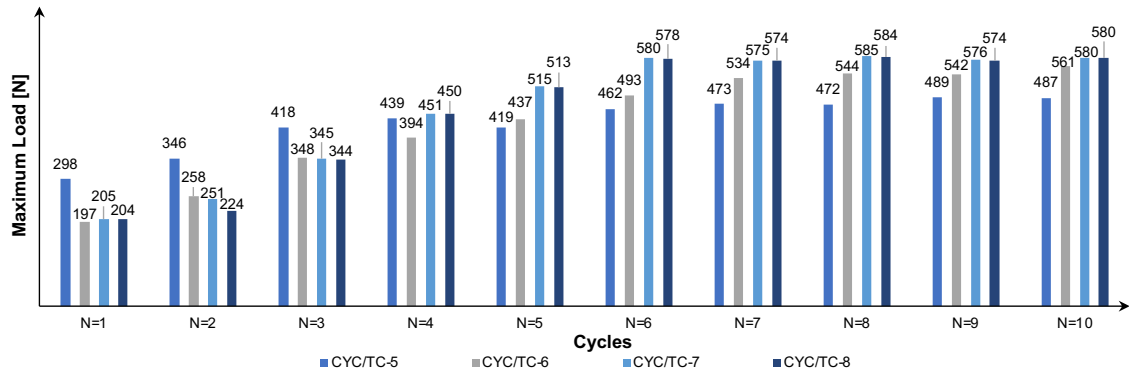


Figure 53 - Variations in maximum attained loads on loose sand

5) Even so, with increasing N , stabilisation appears to be attained around 580 N in last 4 cycles. In Figure 54, it is shown the tendency to stabilisation, especially in the last two tests;

6) In fact, both tests CYC/TC-7 and 8 are so similar that, in Figure 55, their curves for $N = 10$ overlap.

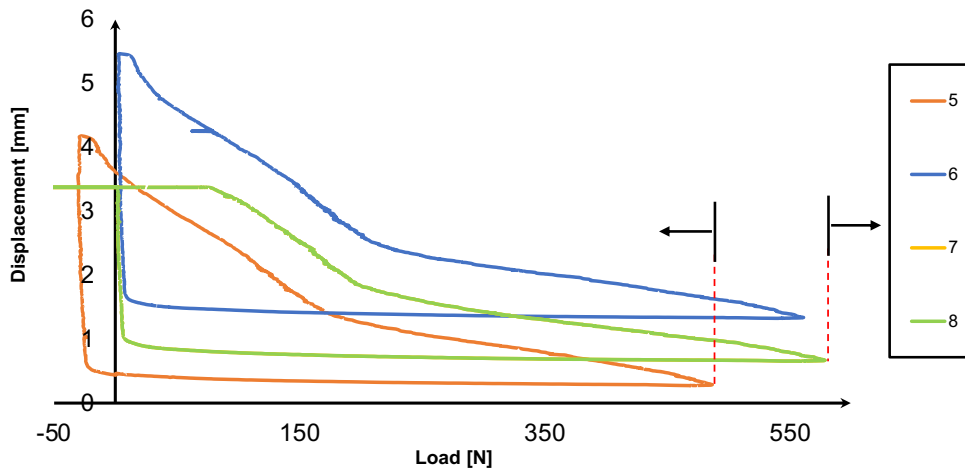


Figure 54 - Load-Displacement at $N = 10$ for tests CYC/TC-5 through 8

Table 14 - Variations in attained loads and displacement on loosen sand preliminary tests

Cycles	Δ Load_compression [N]		Δ Load_tension [N]		Δ displacement [mm]	
	1 \rightarrow 5	5 \rightarrow 10	1 \rightarrow 5	5 \rightarrow 10	1 \rightarrow 5	5 \rightarrow 10
Test #5	124	68	-81	-2	-0.3	-0.1
Test #6	242	123	0	0	-0.6	0.2
Test #7	311	65	0	0	-0.5	-0.1
Test #8	309	66	0	0	-0.2	-0.2

In conclusion, these preliminary tests on the loose *APAS 30* sand are beneficial for further testing, conveying the impression that increasing the number of cycles, N , is favourable in loose soil, since it seems to increase the resistance from cycle to cycle and test to test. The pre-cycling of the soil generally tends to increase the level of stabilisation of the tests as well, having the mobilised resistance stabilised around 580 N. It is discussible whether the last two tests (CYC/TC-7 and 8) are analogous to the first two (CYC/TC-5 and 6), given the discrepancy in imposed displacement. Evidently, this requires further investigation.

6 CONCLUSIONS & RECOMMENDATIONS

6.1 CONCLUSIONS

The aim of this dissertation was to provide relevant knowledge regarding the pile-soil behaviour under cyclic axial loading and the resulting effects with regard to failure, since it has been proven that cyclic loading is very damaging in terms of resistance, as reviewed in many publications. Firstly, a review and summary of previous works was undertaken, highlighting the key points around the cyclic effects on the performance of the pile, including, but not limited to the degradation of the shaft resistance, the number of cycles necessary to failure and the consequent accumulated displacement. It was seen that:

- From publication to publication, the cyclic parameters considered (T , Q_{mean} , Q_{cyclic} , among others) are not consistent, meaning that there is no standardised relevant information when describing the tests performed. In other words, this has a direct negative impact on creating a database with existing tests;
- Even so, from the sample of full and small-scale experimental literature reviewed herein, it was perceived that the initial state of the soil (either dense or loose) is not so important. This may be due to the idea, for cyclic loading, the soil state is consistently being altered from cycle to cycle.

In the pursuit of new discoveries about the unknowns related to cyclic behaviour of piles, the experimental campaign took place. It allowed several evidence to be observed and conjectures to be made, namely:

- In the monotonic tension and compression tests run in loose soil, the behaviour was identical, having resulted in similar failure loads and displacement. The reason for this remains unknown, but two scenarios were questioned: either a large portion of the resistance is being mobilised at the base, or there is none/very little base resistance in compression;
- It was observed the effect of a *two-way* cyclic test, where the pile is pulled out (tension) and pushed in (compression) afterwards. In these compression series, the witnessed behaviour is, in fact, stiffer and therefore capable of attaining higher resistances, than the compression tests where the soil is “intact”. The conjecture made about this was that there is a “new” soil falling to the previous pile position as it is being pulled out. So, when a compression test is performed afterwards, the “new” soil is brutally pushed out of the way, to make room for the pile, hence demonstrating a stiffer behaviour;
- Unexpectedly, the first cycle in tension, in which the soil is still intact, the recorded resistance is less than 50% what had been observed in the monotonic tests, but providing

more equivalent values to the estimation obtained with the EN 1997-1 calculations. Therefore, to fully comprehend the mobilised shaft resistance, further testing would be required;

- Generally speaking, the main difference observed between the two initial soil states considered – dense and loose – was that, while in the dense soil the resistance is higher in the first cycle, it decreases until some stabilisation is achieved. On the other hand, the loose state corresponded to lower resistances in the first cycle, but it keeps increasing until stabilisation is achieved. To sum up, the initial soil state is, in fact, important regarding to the mobilised resistance, contradicting the results found in the literature, in this case;

- Considering the very limited number of cycles tested, i.e. 3 and 10 cycles, it could be anticipated that pre-cycling is beneficial in the sense that, although there might be a loss in resistance (especially in dense conditions), a stabilisation of the resistances with further cycling appears to take place, helping with the prediction of the cyclic pile-soil behaviour;

- The quick degradation of the mobilised shaft resistance is well observed, being almost all dissipated within the first cycle;

- The accuracy and poor performance of the test setup used was also a considerable hindrance, especially, the Stepper Motor. Even after the calibration of the displacement transducer, the induced displacements did not match with the ones commanded to the Motor. Naturally, 1 or 2 mm would not have an impact on a full-scale testing, however, on a small-scale testing, it is no longer true.

Confronted by the fact that the results could be, evidently, improved, further testing was attempted to be run. However, the equipment turned out to be faulty and fixing/replacement was not possible in the remaining time available for the work.

All things considered, the experimental campaign had an adequate start and seemed to be promising, until the motor started to show it was possibly faulty, impeding further testing. Evidently, further experimental testing should have taken place in order to comprehend some suspicions and reservations that were left unanswered.

6.2 RECOMMENDATIONS FOR FUTURE WORK

Evidently, every work has its flaws, ups and downs, and this one is no exception. It was recognised that, in cyclic tests, the aim of always starting in tension was not completely satisfactory, hence the first cycle could have also been in compression, which would alter the load-displacement curve shape.

Another fact is that only *two-way* cyclic tests were run, that is, no *one-way* tests, either in tension or compression, were run, which would be helpful to further understand the cyclic

behaviour. Additionally, although the period of cyclic loading was relatively high comparing to the existing experimental evidence, increasing the number of cycles N could also have been approached.

Since this was a displacement-controlled testing, it would be interesting to run more tests in a load-controlled testing environment instead. This way, the load would be the controllable variable, instead of the displacement.

Lastly and among the other important recommendations is that, when running experimental tests, the acquired data should be interpreted right away, instead of collecting it (sometimes too many) and keeping it to analyse later on. In the present case, should the author have noticed the motor was malfunctioning earlier, the problem could have been addressed in time and further testing would have occurred.

All things considered, and despite the unforeseen, it was considered that this dissertation helped better understanding the cyclic behaviour of the pile-soil system, even if further investigation seems to be required.

REFERENCES

- Achmus, M., Kuo, Y. S., Abdel-Rahman, K., Tseng, Y. H., & Pang, I. (2020). Capacity degradation method for piles under cyclic axial loads. *Computers and Geotechnics*, 128(June), 103838. <https://doi.org/10.1016/j.compgeo.2020.103838>
- Andersen, K., Puech, A., & Jardine, R. (2013). Cyclic resistant geotechnical design and parameter selection for offshore engineering and other applications. TC 209 Workshop 18th ICSMGE: Desing for Cyclic Loading: Piles and Other Foundations, September, 9–44.
- ASTM D2487-17 (2017) Standard Practice for Classification of Soils for Engineering Purposes (Unified Soil Classification System)
- ASTM D4254-16 Standard Test Methods for Minimum Index Density and Unit Weight of Soils and Calculation of Relative Density.
- Blanc, M., Thorel, L., Isorna, R., Dano, C., Kotronis, P., & Philippe, M. (2015). Centrifuge investigation of the axial cyclic behaviour of a single pile used for the foundation of a jacket type offshore wind turbine. In *Frontiers in Offshore Geotechnics III* (pp. 521–526). CRC Press. <https://doi.org/10.1201/b18442-65>
- Brandl, H. (2006). Energy foundations and other thermo-active ground structures. *Geotechnique*, 56(2), 81–122. <https://doi.org/10.1680/geot.2006.56.2.81>
- BS 1377-4:1990 Methods of test for soils for civil engineering purposes - Compaction-related tests
- CEN (European Committee for Standardization), "Eurocode 7: Geotechnical design – Part 1: General Rules", EN 1997-1. Brussels, Belgium, 2010.
- DeJong, Jason Randolph, Mark White, D. (2003). NII-Electronic Library Service. Japanese Geotechnical Society, *Soils and Foundations*, 43, 2091.
- Dithinde, M., Phoon, K. K., De Wet, M., & Retief, J. V. (2011). Characterization of Model Uncertainty in the Static Pile Design Formula. *Journal of Geotechnical and Geoenvironmental Engineering*, 137(1), 70–85. [https://doi.org/10.1061/\(asce\)gt.1943-5606.0000401](https://doi.org/10.1061/(asce)gt.1943-5606.0000401)
- E 239-1970 (1970) Solos - Análise Granulométrica Por Peneiração Húmida, Laboratório Nacional de Engenharia Civil, Portugal

- Fellenius, B. H. (2007). Discussion: Behaviour of jacked and driven piles in sandy soil. *Geotechnique*, 57(5), 475–478. <https://doi.org/10.1680/geot.2007.57.5.475>
- Fioravante, V. (2002). On the Shaft Friction Modelling of Non-displacement Piles in Sand. Japanese Geotechnical Society, in *Soils and Foundations*, p. 42(2), 23–33.
- Fleming, K., Weltman, A., Randolph, M., & Elson, K. (2009). *Piling Engineering* (3rd ed.). CRC Press. <https://doi.org/10.1201/b22272>
- Garnier, J., Gaudin, C., Springman, S. M., Culligan, P. J., Goodings, D., König, D., Kutter, B., Phillips, R., Randolph, M. F., & Thorel, L. (2007). Catalogue of scaling laws and similitude questions in geotechnical centrifuge modelling. *International Journal of Physical Modelling in Geotechnics*, 7(3), 01–23.
- Gavin, K., Cadogan, D., & Twomey, L. (2008). Axial resistance of CFA piles in Dublin Boulder Clay. *Proceedings of the Institution of Civil Engineers: Geotechnical Engineering*, 161(4), 171–180. <https://doi.org/10.1680/geng.2008.161.4.171>
- Gavin, K., Igoe, D., & Doherty, P. (2011). Piles for offshore wind turbines: A state-of-the-art review. *Proceedings of the Institution of Civil Engineers: Geotechnical Engineering*, 164(4), 245–256. <https://doi.org/10.1680/geng.2011.164.4.245>
- El Haffar, I. (2018). Physical modeling and study of the behavior of deep foundations of offshore wind turbines in sand. (Doctoral Thesis, École centrale de Nantes, France).
- Li, B. (2019). Study on the strength influence of pile driving disturbance on the surrounding soil. *E3S Web of Conferences*, 136, 8–10. <https://doi.org/10.1051/e3sconf/201913604078>
- Li, Z., Bolton, M. D., & Haigh, S. K. (2012). Cyclic axial behaviour of piles and pile groups in sand. *Canadian Geotechnical Journal*, 49(9), 1074–1087. <https://doi.org/10.1139/T2012-070>
- NP 83 - 65 (1965) Solos - Determinação da Densidade das Partículas, Laboratório Nacional de Engenharia Civil, Portugal
- Patel, R. (2011). Behaviour of Tension Piles under Cyclic Loading (Masters Dissertation, Leibniz Universität Hannover, Germany). <https://doi.org/10.13140/RG.2.2.21476.32641>
- Poulos, H. G. (1991). Cyclic axial loading analysis of piles in sand. *Journal of Geotechnical Engineering*, 117(9), 1438–1440. [https://doi.org/10.1061/\(ASCE\)0733-9410\(1991\)117:9\(1438\)](https://doi.org/10.1061/(ASCE)0733-9410(1991)117:9(1438))

- Puech, A., & Garnier, J. (2017). Design of Piles Under Cyclic Loading. In A. Puech & J. Garnier (Eds.), *Design of Piles Under Cyclic Loading: SOLCYP Recommendations*. John Wiley & Sons, Inc. <https://doi.org/10.1002/9781119469018>
- Santos, J. A. (2008). *Fundações por Estacas - Acções Verticais*. *Obras Geotécnicas-Elementos Teóricos*. Instituto Superior Técnico, 55.
- Sutman, M., Speranza, G., Ferrari, A., Larrey-Lassalle, P., & Laloui, L. (2020). Long-term performance and life cycle assessment of energy piles in three different climatic conditions. *Renewable Energy*, 146, 1177–1191. <https://doi.org/10.1016/j.renene.2019.07.035>
- Tomlinson, M., & Woodward, J. (2007). *Pile Design and Construction Practice* (5th ed.). CRC Press. <https://doi.org/10.4324/9780203964293>
- Yasufuku, N., Ochiai, H., & Ohno, S. (2001). Pile end-bearing capacity of sand related to soil compressibility. *Soils and Foundations*, 41(4), 59–71. https://doi.org/10.3208/sandf.41.4_59

APPENDICES

APPENDIX A – CHECKLIST FOR RUNNING THE TESTS

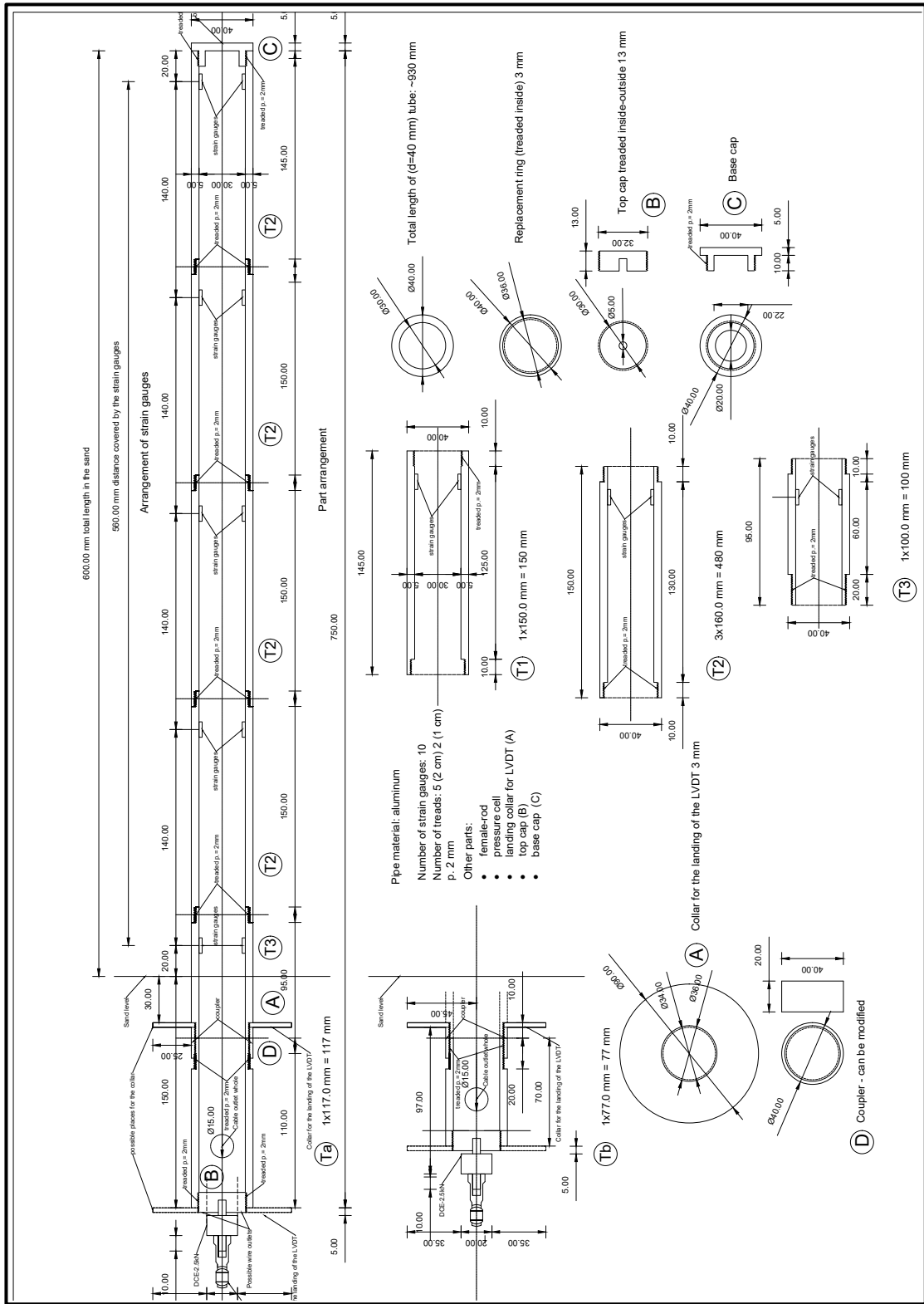
CHECKLIST FOR RUNNING LOAD TESTS

1. Place the pile, load cell and displacement transducer;
2. Fill the tank up with the soil, accordingly;
3. On the computer, run the datalogger *InstruNet* software:
 - Check the *Recording Options* as:

The screenshot shows the 'Record Setup' dialog box in the InstruNet software. It is divided into several sections: 'Digitize' (Points Per Scan: 1000000, Number of Scans: 1, Sample Rate: 20.000, Scan Mode: Oscilloscope), 'Display' (Horiz Scale: Auto, Horiz Label: Relative Time, Min Disp Height: 40, Plot: Lines), 'Storage' (Digitize Into: To Ram Buffer, File Type: Binary), and 'Auto Afs' (Off). There are also buttons for 'Trigger...', 'Timing...', 'Record...', 'Window...', 'Calibration...', 'More...', 'Cancel', and 'OK'.

- Load Cell – Ch. 11 (Labels upside down)
 - + Compression
 - Tension
 - Displacement Transducer – Ch. 15
 - + Tension
 - Compression
 - Press *Record*
4. Run the *MacTalk* software to control the motor:
 - 409600 motor counts = 5 mm displacement
 - After setting the no. of counts, press *Reset Position*
 - Press *Start*
 - + Compression
 - Tension
 5. After the test, click on *Save Waveforms to Excel*

APPENDIX B – SMALL SCALE PILE SCHEMATIC VIEW AND DIMENSIONS



APPENDIX C – APAS 30 SUPPLIER TECHNICAL SHEET



1515-CPR-0205



13

DECLARAÇÃO DE DESEMPENHO

Nº 5/2013

- Código de identificação único do produto-tipo: **Agregado 0/1**
- Descrição do produto-tipo: **Refª APAS 30 (registo na guia de remessa)**
Areia com presença de minerais de quartzito, quartzo e feldspato. Partículas de forma subprismática, subangulosa e com superfície ligeiramente rugosa.
- Utilização ou utilizações previstas do produto de construção, de acordo com a especificação técnica harmonizada aplicável, tal como previsto pelo fabricante: **EN 13139:2002; EN 13139:2002/AC:2004 (agregado para argamassas).**
- Nome, designação comercial ou marca comercial registada e endereço de contacto do fabricante, nos termos do nº 5 do artigo 11º:
Areipor - Areias Portuguesas, Lda. Rua da Alameda, Ap 755 - 2671-601 Bucelas
E-mail: geral@areipor.mail.pt Telefone: 21 968 80 10 Fax: 21 968 80 19
- Sistema ou sistemas de avaliação e verificação da regularidade do desempenho do produto de construção tal como previsto no anexo V:
Sistema de avaliação 2+
- No caso de uma declaração de desempenho relativa a um produto de construção abrangido por uma norma harmonizada:
E.I.C. - Empresa Internacional de Certificação, organismo notificado, nº 1515, realizou a inspeção inicial e o acompanhamento, apreciação e aprovação contínuos do controlo da produção em fábrica, no âmbito do sistema 2+, e emitiu o certificado de conformidade nº 1515-CPD-0205 de 30 de maio de 2013 e substituído pelo certificado de conformidade nº 1515-CPR-0205 de 21 de fevereiro de 2018, válido até 30 de março de 2021, desde que não se alterem significativamente as condições definidas nas normas harmonizadas ou as condições de fabrico e do controlo de produção em fábrica.

7. Desempenho declarado


Norma harmonizada	EN 13139:2002	EN 13139:2002/AC:2004
Características	Desempenho	
Dimensão Nominal - Tamanho das partículas	0/1	
Massa Volúmica* (Mg/m ³)	$\rho_a = 2,61 - 2,71$ $\rho_{rd} = 2,58 - 2,68$ $\rho_{std} = 2,59 - 2,69$	Granulometria típica
Absorção de água*	< 0,9%	Abertura (mm)
Teor de finos	Categoria 1	(%)
Teor de cloretos	< 0,01%	Tolerância (%)
Teor de sulfatos solúveis em ácido	AS _{0,2}	2
Teor de enxofre total	< 0,1%	1
Teor de húmus	Mais claro que padrão	0,250
		2
		0,063
		0,0
		0,0-5,0

Notas: Resultados que não constam, não foram realizados ou não solicitados.
 A origem dos valores dos ensaios químicos são da responsabilidade do produtor da matéria-prima.
 Mais informações disponível na Ficha de Dados de Segurança

- O desempenho do produto identificado nos pontos 1 e 2 é conforme com o desempenho declarado no ponto 7.
 A presente declaração de desempenho é emitida em conformidade com o Regulamento (UE) nº 305/2011 sob a exclusiva responsabilidade do fabricante identificado no ponto 4.

Assinado por e em nome do fabricante por:

Miguel Miranda, Administrador


 (assinatura)

Bucelas, 13 abril 2018

APPENDIX D – PARTICLE SIZE TESTING (STANDARD E 239)

UNIVERSIDADE DE LISBOA
INSTITUTO SUPERIOR TÉCNICO
DECIVIL



LABORATÓRIO DE GEOTECNIA

ANÁLISE GRANULOMÉTRICA
LNEC - E 239

REFERÊNCIA: SMALL-SCALE MODEL: SANTIAGO PINTO DATA: 20/07/21

AMOSTRA: _____ PROFUNDIDADE: _____
Massa total da amostra mt (g)= 100.00
Massa retida no peneiro de 2.00 mm (# 10) m_{10} (g)= 100.00
Massa passada no peneiro de 2.00 mm (# 10) m'_{10} (g)= 100.00

FRACÇÃO RETIDA NO PENEIRO DE 2.00 mm (# 10)

PENEIROS	MASSA RETIDA (g) m_x	% RETIDA $N_x=100 m_x / mt$	%ACU. RETIDA N'_x	%ACU. PASSA $N''_x=100 - N'_x$
50.0 (2")	0.00	0.00	0.00	100.00
37.5 (3/2")	0.00	0.00	0.00	100.00
25.0 (1")	0.00	0.00	0.00	100.00
19.0 (3/4")	0.00	0.00	0.00	100.00
9.5 (3/8")	0.00	0.00	0.00	100.00
4.75 (# 4)	0.00	0.00	0.00	100.00
2.00 (# 10)	0.00	0.00	0.00	100.00

FRACÇÃO PASSADA NO PENEIRO DE 2.00mm (# 10)

Massa da amostra a ensaiar		ma (g)= 100.00		
		$N'_{10}=100 (m'_{10}/mt) = 100.00$		
PENEIROS	MASSA RETIDA (g) m_x	% RETIDA $N_x= (m_x / ma) N'_{10}$	%ACU. RETIDA N'_x	%ACU. PASSA $N''_x=100 - N'_x$
20	1.50	1.50	1.50	98.50
40	87.20	87.20	88.70	11.30
60	10.50	10.50	99.20	0.80
140	0.50	0.50	99.70	0.30
200	0.00	0.00	99.70	0.30

APPENDIX E – PARTICLE DENSITY TESTING

UNIVERSIDADE DE LISBOA
INSTITUTO SUPERIOR TÉCNICO
DECIVIL



LABORATÓRIO DE GEOTECNIA

DENSIDADE DAS PARTÍCULAS

NP-83 (1965)

AMOSTRA SMALL-SCALE MODEL: SANTIAGO PINTO DATA: 20/07/21

		Número do Picnómetro			
			86	76	96
	Cápsula				
A	Massa de cápsula	g	97.72	109.58	15.80
B	Massa do solo + cápsula	g	122.82	134.54	40.73
m4 = B - A	Massa de solo seco	g	25.10	24.96	24.93
m5	Massa do picnómetro + água + solo	g	150.21	151.66	149.32
t	Temperatura do ensaio	°C	24.00	24.00	24.00
m3	Massa do picnómetro cheio de água à temperatura (t)	g	134.51	136.10	133.81
K	Quociente entre a densidade da água à temperatura t e 20°C		1.00	1.00	1.00
$d = K \times m4 / (m3 - m5 + m4)$	Densidade das partículas		2.67	2.66	2.65

Observações

Gs= 2.66